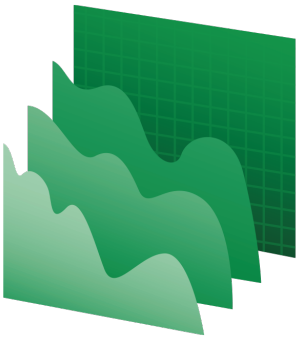

Match-up database Analyses Report

Aquarius-L3-JPL-V5-MONTHLY

TSG-LEGOS-DM

Sea of Japan

prepared by the Pi-MEP Consortium

September 15, 2019

Contents

1 Overview **6**

2 The MDB file datasets **7**
2.1 Satellite SSS product . . . 7
2.1.1 Aquarius-L3-JPL-V5-MONTHLY . . . 7
2.2 *In situ* SSS dataset . . . 7
2.3 Auxiliary geophysical datasets . . . 8
2.3.1 CMORPH . . . 8
2.3.2 ASCAT . . . 9
2.3.3 ISAS . . . 9
2.3.4 World Ocean Atlas Climatology . . . 10
2.4 Overview of the Match-ups generation method . . . 10
2.4.1 *In situ*/Satellite data filtering . . . 10
2.4.2 *In situ*/Satellite Co-localization . . . 10
2.4.3 MDB pair Co-localization with auxiliary data and complementary information . . . 11
2.4.4 Content of the Match-Up NetCDF files . . . 12
2.5 MDB characteristics for the particular *in situ*/satellite pairs . . . 18
2.5.1 Number of paired SSS data as a function of time and distance to coast . . . 18
2.5.2 Histograms of the SSS match-ups . . . 18
2.5.3 Distribution of *in situ* SSS depth measurements . . . 19
2.5.4 Spatial Distribution of Match-ups . . . 20
2.5.5 Histograms of the spatial and temporal lags of the match-ups pairs . . . 21

3 MDB file Analyses **21**
3.1 Spatial Maps of the Temporal mean and Std of *in situ* and satellite SSS and of the difference (ΔSSS) . . . 21
3.2 Time series of the monthly median and Std of *in situ* and satellite SSS and of the (ΔSSS) . . . 23
3.3 Zonal mean and Std of *in situ* and satellite SSS and of the ΔSSS . . . 23
3.4 Scatterplots of satellite vs *in situ* SSS by latitudinal bands . . . 25
3.5 Time series of the monthly median and Std of the ΔSSS sorted by latitudinal bands 26
3.6 ΔSSS sorted as function of geophysical parameters . . . 26
3.7 ΔSSS maps and statistics for different geophysical conditions . . . 27

4 Summary **30**

5 More Comparison/Validation Materials **32**
5.1 Comparisons with other satellite products . . . 32
5.2 Statistics derived for the different *in situ* databases . . . 34

List of Figures

1 Number of match-ups between TSG-LEGOS-DM and Aquarius-L3-JPL-V5-MONTHLY SSS as a function of time (a) and as function of the distance to coast (b) over the Sea of Japan Pi-MEP region and for the full satellite product period. . . . 18

2 Histograms of SSS from TSG-LEGOS-DM (a) and Aquarius-L3-JPL-V5-MONTHLY (b) considering all match-up pairs per bins of 0.1 over the Sea of Japan Pi-MEP region and for the full satellite product period. 18
3 Histograms of the depth of the upper level SSS measurements from TSG-LEGOS-DM in the Match-up DataBase for the Sea of Japan Pi-MEP region (a) and temporal mean spatial distribution of pressure of the *in situ* SSS data over 1°x1° boxes and for the full satellite product period (b). 19
4 Number of SSS match-ups between TSG-LEGOS-DM SSS and the Aquarius-L3-JPL-V5-MONTHLY SSS product for the Sea of Japan Pi-MEP region over 1°x1° boxes and for the full satellite product period. 20
5 Histograms of the spatial (a) and temporal (b) lags between the time of the TSG-LEGOS-DM measurements and the date of the corresponding Aquarius-L3-JPL-V5-MONTHLY SSS product. 21
6 Temporal mean (left) and Std (right) of SSS from Aquarius-L3-JPL-V5-MONTHLY (top), TSG-LEGOS-DM (middle), and of ΔSSS (Satellite - TSG-LEGOS-DM). Only match-up pairs are used to generate these maps. 22
7 Time series of the monthly median SSS (top), median of ΔSSS (Satellite - TSG-LEGOS-DM) and Std of ΔSSS (Satellite - TSG-LEGOS-DM) over the Sea of Japan Pi-MEP region considering all match-ups collected by the Pi-MEP. 23
8 Left panel: Zonal mean SSS from Aquarius-L3-JPL-V5-MONTHLY satellite product (black) and from TSG-LEGOS-DM (blue). Right panel: Zonal mean of ΔSSS (Satellite - TSG-LEGOS-DM) for all the collected Pi-MEP match-up pairs estimated over the full satellite product period. 24
9 Contour maps of the concentration of Aquarius-L3-JPL-V5-MONTHLY SSS (y-axis) versus TSG-LEGOS-DM SSS (x-axis) at match-up pairs for different latitude bands. For each plot, the red line shows x=y. The black thin and dashed lines indicate a linear fit through the data cloud and the ±95% confidence levels, respectively. The number match-up pairs n, the slope and R^2 coefficient of the linear fit, the root mean square (RMS) and the mean bias between satellite and *in situ* data are indicated for each latitude band in each plots. 25
10 Monthly median (red curves) of ΔSSS (Satellite - TSG-LEGOS-DM) and ±1 Std (black vertical thick bars) as function of time for all the collected Pi-MEP match-up pairs estimated over the Sea of Japan Pi-MEP region and for the full satellite product period are shown for different latitude bands: (a) 80°S-80°N, (b) 20°S-20°N, (c) 40°S-20°S and 20°N-40°N and (d) 60°S-40°S and 40°N-60°N. 26
11 ΔSSS (Satellite - TSG-LEGOS-DM) sorted as function of TSG-LEGOS-DM SSS values a), TSG-LEGOS-DM SST b), ASCAT Wind speed c), CMORPH rain rate d), distance to coast (e) and *in situ* measurement depth (f). In all plots the median and Std of ΔSSS for each bin is indicated by the red curves and black vertical thick bars (±1 Std) 27
12 Temporal mean gridded over spatial boxes of size 1°x1° of ΔSSS (Aquarius-L3-JPL-V5-MONTHLY - TSG-LEGOS-DM) for 5 different subdatasets corresponding to:RR=0 mm/h, 3< U_{10} <12 m/s, SST>5°C, distance to coast > 800 km (a), RR=0 mm/h, 3< U_{10} <12 m/s (b), RR>1mm/h and U_{10} <4m/s (c), WOA2013 SSS Std<0.2 (d), WOA2013 SSS Std>0.2 (e). 29

13 Normalized histogram of ΔSSS (Aquarius-L3-JPL-V5-MONTHLY - TSG-LEGOS-DM) for 5 different subdatasets corresponding to: RR=0 mm/h, 3< U_{10} <12 m/s, SST>5°C, distance to coast > 800 km (a), RR=0 mm/h, 3< U_{10} <12 m/s (b), RR>1mm/h and U_{10} <4m/s (c), WOA2013 SSS Std<0.2 (d), WOA2013 SSS Std>0.2 (e). 30

Acronym

Aquarius	NASA/CONAE Salinity mission
ASCAT	Advanced Scatterometer
ATBD	Algorithm Theoretical Baseline Document
BLT	Barrier Layer Thickness
CMORPH	CPC MORPHing technique (precipitation analyses)
CPC	Climate Prediction Center
CTD	Instrument used to measure the conductivity, temperature, and pressure of seawater
DM	Delayed Mode
EO	Earth Observation
ESA	European Space Agency
FTP	File Transfer Protocol
GOSUD	Global Ocean Surface Underway Data
GTMBA	The Global Tropical Moored Buoy Array
Ifremer	Institut français de recherche pour l'exploitation de la mer
IPEV	Institut polaire français Paul-Émile Victor
IQR	Interquartile range
ISAS	*In Situ* Analysis System
Kurt	Kurtosis (fourth central moment divided by fourth power of the standard deviation)
L2	Level 2
LEGOS	Laboratoire d'Etudes en Géophysique et Océanographie Spatiales
LOCEAN	Laboratoire d'Océanographie et du Climat : Expérimentations et Approches Numériques
LOPS	Laboratoire d'Océanographie Physique et Spatiale
MDB	Match-up Data Base
MEOP	Marine Mammals Exploring the Oceans Pole to Pole
MLD	Mixed Layer Depth
NCEI	National Centers for Environmental Information
NRT	Near Real Time
NTAS	Northwest Tropical Atlantic Station
OI	Optimal interpolation
Pi-MEP	Pilot-Mission Exploitation Platform
PIRATA	Prediction and Researched Moored Array in the Atlantic
QC	Quality control
R_{sat}	Spatial resolution of the satellite SSS product
RAMA	Research Moored Array for African-Asian-Australian Monsoon Analysis and Prediction
r^2	Square of the Pearson correlation coefficient
RMS	Root mean square
RR	Rain rate
SAMOS	Shipboard Automated Meteorological and Oceanographic System
Skew	Skewness (third central moment divided by the cube of the standard deviation)
SMAP	Soil Moisture Active Passive (NASA mission)
SMOS	Soil Moisture and Ocean Salinity (ESA mission)
SPURS	Salinity Processes in the Upper Ocean Regional Study
SSS	Sea Surface Salinity
SSS_{insitu}	*In situ* SSS data considered for the match-up

SSS_{SAT}	Satellite SSS product considered for the match-up
ΔSSS	Difference between satellite and *in situ* SSS at colocalized point (ΔSSS = SSS_{SAT}- SSS_{insitu})
SST	Sea Surface Temperature
Std	Standard deviation
Std*	Robust Standard deviation = median(abs(x-median (x)))/0.67 (less affected by outliers than Std)
Stratus	Surface buoy located in the eastern tropical Pacific
Survostral	SURVeillance de l'Océan AuSTRAL (Monitoring the Southern Ocean)
TAO	Tropical Atmosphere Ocean
TSG	ThermoSalinoGraph
WHOI	Woods Hole Oceanographic Institution
WHOTS	WHOI Hawaii Ocean Time-series Station
WOA	World Ocean Atlas

1 Overview

In this report, we present systematic analyses of the Match-up DataBase (MDB) files generated by the Pi-MEP platform within the following Pi-MEP region and for the below pair of Satellite/*in situ* SSS data:

- Pi-MEP region: Sea of Japan (download the corresponding mask in NetCDF here)
- SSS satellite product (SSS_{SAT}): Aquarius-L3-JPL-V5-MONTHLY
- *In situ* dataset (SSS_{Insitu}): TSG-LEGOS-DM (download the corresponding *in situ* report here)

In the following, $\Delta SSS = SSS_{SAT} - SSS_{Insitu}$ denotes the difference between the satellite and *in situ* SSS at the colocalized points that form the MDB.

This report presents successively:

The MDB file DataSets (Section 2)

- A short description of the satellite SSS product considered in the match-up (2.1)
- A short description of the *in situ* SSS dataset considered in the match-up (2.2)
- A short description of the auxiliary geophysical datasets co-localized with SSS pairs (2.3)
- An overview of how the Match-ups were evaluated (2.4)
- An overview of the MDB characteristics for the particular *in situ*/satellite pairs (2.5)

The major results of the MDB file Analyses (Section 3)

- Spatial Maps of the Time-mean and temporal Std of *in situ* and satellite SSS and of the ΔSSS (3.1)
- Time series of the monthly median and Std of *in situ* and satellite SSS and of the ΔSSS (3.2)
- Zonal mean and Std of *in situ* and satellite SSS and of the ΔSSS (3.3)
- Scatterplots of satellite vs *in situ* SSS by latitudinal bands (3.4)
- Time series of the monthly median and Std of the ΔSSS sorted by latitudinal bands (3.5)
- ΔSSS sorted as function of geophysical parameters (3.6)
- ΔSSS maps and statistics for different geophysical conditions (3.7)

All analyses are conducted over the Pi-MEP Region specified above and over the full satellite SSS product period. Original figures appearing in this report can be downloaded as PNG files here or by clicking directly on the figure.

2 The MDB file datasets

2.1 Satellite SSS product

2.1.1 Aquarius-L3-JPL-V5-MONTHLY

Version 5.0 Aquarius CAP Level 3 products are the fourth release of the AQUARIUS/SAC-D mapped salinity and wind speed data based on the Combined Active Passive (CAP) algorithm. Level 3 standard mapped image products contain gridded 1 degree spatial resolution salinity and wind speed data averaged over 7 day and monthly time scales. This particular data set is the monthly mean sea surface salinity (SSS) V5.0 Aquarius CAP product. CAP is a P.I. produced data set developed and provided by JPL. The CAP algorithm utilizes data from both the on-board radiometer and scatterometer to simultaneously retrieve salinity, wind speed and direction by minimizing the sum of squared differences between model and observations. The main improvements in CAP V5.0 relative to the previous version include: updates to the Geophysical Model Functions to 4th order harmonics with the inclusion of sea surface temperature (SST) and stability at air-sea interface effects; use of the Canadian Meteorological Center (CMC) SST product as the new source ancillary sea surface temperature data in place of NOAA OI SST. The Aquarius instrument is onboard the AQUARIUS/SAC-D satellite, a collaborative effort between NASA and the Argentinian Space Agency Comision Nacional de Actividades Espaciales (CONAE). The instrument consists of three radiometers in push broom alignment at incidence angles of 29, 38, and 46 degrees incidence angles relative to the shadow side of the orbit. Footprints for the beams are: 76 km (along-track) x 94 km (cross-track), 84 km x 120 km and 96km x 156 km, yielding a total cross-track swath of 370 km. The radiometers measure brightness temperature at 1.413 GHz in their respective horizontal and vertical polarizations (TH and TV). A scatterometer operating at 1.26 GHz measures ocean backscatter in each footprint that is used for surface roughness corrections in the estimation of salinity. The scatterometer has an approximate 390km swath.

Table 1: Satellite SSS product characteristics

Aquarius-L3-JPL-V5-MONTHLY	
Spatial resolution	1°x1°
Temporal repeat	Monthly
Temporal coverage	From 2011-08-25 to 2015-06-07
Spatial coverage	Global [-180 180 -90 90]
Data Provider	Simon Yueh at Jet Propulsion Laboratory, Pasadena, USA
Release Date	2018-10-01
Version	5
User Guide	Aquarius-CAP-User-Guide-v5.0.pdf
Documentation	ftp://podaac-ftp.jpl.nasa.gov/allData/aquarius/docs/CAPv5/
DOI	http://dx.doi.org/10.5067/AQR50-3TMCS

2.2 *In situ* SSS dataset

The TSG-LEGOS-DM dataset correspond to sea surface salinity delayed mode data derived from voluntary observing ships collected, validated, archived, and made freely available by the French Sea Surface Salinity Observation Service (Alory et al. (2015)). Adjusted values when available and only collected TSG data that exhibit quality flags=1 and 2 were used.

2.3 Auxiliary geophysical datasets

Additional EO datasets are used to characterize the geophysical conditions at the *in situ*/satellite SSS pair measurement locations and time, and 10 days prior the measurements to get an estimate of the geophysical condition and history. As discussed in Boutin et al. (2016), the presence of vertical gradients in, and horizontal variability of, sea surface salinity indeed complicates comparison of satellite and *in situ* measurements. The additional EO data are used here to get a first estimates of conditions for which L-band satellite SSS measured in the first centimeters of the upper ocean within a 50-150 km diameter footprint might differ from pointwise *in situ* measurements performed in general between 10 and 5 m depth below the surface. The spatio-temporal variability of SSS within a satellite footprint (50–150 km) is a major issue for satellite SSS validation in the vicinity of river plumes, frontal zones, and significant precipitation. Rainfall can in some cases produce vertical salinity gradients exceeding 1 pss m^{-1}; consequently, it is recommended that satellite and *in situ* SSS measurements less than 3–6 h after rain events should be considered with care when used in satellite calibration/validation analyses. To identify such situation, the Pi-MEP platform is first using CMORPH products to characterize the local value and history of rain rate and ASCAT gridded data are used to characterize the local surface wind speed and history. For validation purpose, the ISAS monthly SSS *in situ* analysed fields at 5 m depth are collocated and compared with the satellite SSS products. The use of ISAS is motivated by the fact that it is used in the SMOS L2 official validation protocol in which systematic comparisons of SMOS L2 retrieved SSS with ISAS are done. In complement to ISAS, monthly std climatological fields from the World Ocean Atlas (WOA13) at the match-up pairs location and date are also used to have an a priori information of the local SSS variability.

2.3.1 CMORPH

Precipitation are estimated using the CMORPH 3-hourly products at 1/4° resolution (Joyce et al. (2004)). CMORPH (CPC MORPHing technique) produces global precipitation analyses at very high spatial and temporal resolution. This technique uses precipitation estimates that have been derived from low orbiter satellite microwave observations exclusively, and whose features are transported via spatial propagation information that is obtained entirely from geostationary satellite IR data. At present NOAA incorporate precipitation estimates derived from the passive microwaves aboard the DMSP 13, 14 and 15 (SSM/I), the NOAA-15, 16, 17 and 18 (AMSU-B), and AMSR-E and TMI aboard NASA's Aqua, TRMM and GPM spacecraft, respectively. These estimates are generated by algorithms of Ferraro (1997) for SSM/I, Ferraro et al. (2000) for AMSU-B and Kummerow et al. (2001) for TMI. Note that this technique is not a precipitation estimation algorithm but a means by which estimates from existing microwave rainfall algorithms can be combined. Therefore, this method is extremely flexible such that any precipitation estimates from any microwave satellite source can be incorporated.

With regard to spatial resolution, although the precipitation estimates are available on a grid with a spacing of 8 km (at the equator), the resolution of the individual satellite-derived estimates is coarser than that - more on the order of 12 x 15 km or so. The finer "resolution" is obtained via interpolation.

In effect, IR data are used as a means to transport the microwave-derived precipitation features during periods when microwave data are not available at a location. Propagation vector matrices are produced by computing spatial lag correlations on successive images of geostationary satellite IR which are then used to propagate the microwave derived precipitation estimates. This process governs the movement of the precipitation features only. At a given location, the shape and intensity of the precipitation features in the intervening half hour periods between microwave scans are determined by performing a time-weighting interpolation between microwave-derived

features that have been propagated forward in time from the previous microwave observation and those that have been propagated backward in time from the following microwave scan. NOAA refer to this latter step as "morphing" of the features.

For the present Pi-MEP products, we only considered the 3-hourly products at 1/4 degree resolution. The entire CMORPH record (December 2002-present) for 3-hourly, 1/4 degree lat/lon resolution can be found at: ftp://ftp.cpc.ncep.noaa.gov/precip/CMORPH_V1.0/CRT/. CMORPH estimates cover a global belt (-180°W to 180°E) extending from 60°S to 60°N latitude and are available for the complete period of the Pi-MEP core datasets (Jan 2010-now).

2.3.2 ASCAT

Advanced SCATterometer (ASCAT) daily data produced and made available at Ifremer/CERSAT on a 0.25°x0.25° resolution grid (Bentamy and Fillon (2012)) since March 2007 are used to characterize the mean daily wind at the match-up pair location as well as the wind history during the 10-days period preceding the in situ measurement date. These wind fields are calculated based on a geostatistical method with external drift. Remotely sensed data from ASCAT are considered as observations while those from numerical model analysis (ECMWF) are associated with the external drift. The spatial and temporal structure functions for wind speed, zonal and meridional wind components are estimated from ASCAT retrievals. Furthermore, the new procedure includes a temporal interpolation of the retrievals based on the complex empirical orthogonal function (CEOF) approach, in order to enhance the sampling length of the scatterometer observations. The resulting daily wind fields involves the main known surface wind patterns as well as some variation modes associated with temporal and spatial moving features. The accuracy of the gridded winds was investigated through comparisons with moored buoy data in Bentamy et al. (2012) and resulted in rms differences for wind speed and direction are about 1.50 m.s^{-1} and 20°.

2.3.3 ISAS

The In Situ Analysis System (ISAS), as described in Gaillard et al. (2016) is a data based reanalysis of temperature and salinity fields over the global ocean. It was initially designed to synthesize the temperature and salinity profiles collected by the Argo program. It has been later extended to accommodate all type of vertical profile as well as time series. ISAS gridded fields are entirely based on *in situ* measurements. The methodology and configuration have been conceived to preserve as much as possible the data information content and resolution. ISAS is developed and run in a research laboratory (LOPS) in close collaboration with Coriolis, one of Argo Global Data Assembly Center and unique data provider for the Mercator operational oceanography system. At the moment the period covered starts in 2002 and only the upper 2000 m are considered. The gridded fields were produced over the global ocean 70°N–70°S on a 1/2° grid by the ISAS project with datasets downloaded from the Coriolis data center (for more details on ISAS see Gaillard et al. (2009)). In the Pi-MEP, the product in used is the INSITU_GLO_TS_OA_NRT_OBSERVATIONS_013_002_a v6.2 NRT derived at the Coriolis data center and provided by the Copernicus Marine Environment Monitoring Service (CMEMS). The major contribution to the data set is from Argo array of profiling floats, reaching an approximate resolution of one profile every 10-days and every 3-degrees over the satellite SSS period (http://www.umr-lops.fr/SNO-Argo/Products/ISAS-T-S-fields/); in this version SSS from ship of opportunity thermosalinographs are not used, so that we can consider SMOS SSS validation using these measurements independent of ISAS. The ISAS optimal interpolation involves a structure function modeled as the sum of two Gaussian functions, each associated with specific time and space scales, resulting in a smoothing over typically 3 degrees. The smallest scale which can

be retrieved with ISAS analysis is not smaller than 300–500 km (Kolodziejczyk et al. (2015)). For validation purpose, the ISAS monthly SSS fields at 5 m depth are collocated and compared with the satellite SSS products and included in the Pi-MEP Match-up files. In addition, the "percentage of variance" fields (PCTVAR) contained in the ISAS analyses provide information on the local variability of *in situ* SSS measurements within 1/2°x1/2° boxes.

2.3.4 World Ocean Atlas Climatology

The World Ocean Atlas 2013 version 2 (WOA13 V2) is a set of objectively analyzed (1° grid) climatological fields of *in situ* temperature, salinity and other variables provided at standard depth levels for annual, seasonal, and monthly compositing periods for the World Ocean. It also includes associated statistical fields of observed oceanographic profile data interpolated to standard depth levels on 5°, 1°, and 0.25° grids. We use these fields in complement to ISAS to characterize the climatological fields (annual mean and std) at the match-up pairs location and date.

2.4 Overview of the Match-ups generation method

The match-up production is basically a three steps process:

1. preparation of the input *in situ* and satellite data, and,
2. co-localization of satellite products with *in situ* SSS measurements.
3. co-localization of the *in situ*/satellite pair with auxiliary information.

In the following, we successively detail the approaches taken for these different steps.

2.4.1 *In situ*/Satellite data filtering

The first step consists in filtering TSG-LEGOS-DM *in situ* data using the quality flags as described in 2.2 so that only valid salinity data remain in the final match-up files.

For high-spatial resolution *in situ* SSS measurements such as the Thermo-SalinoGraph (TSG) SSS data, as well as SSS data from surface drifters, an additional spatial filtering step is performed on the *in situ* data that will be in fine compared to the satellite SSS products. If R_{sat} is the spatial resolution of the satellite SSS product (L2 to L3-L4), the *in situ* data are spatially low pass filtered using a running median filter with a window width=R_{sat} to try to minimize the spatial representativeness uncertainty when comparing to the lower spatial resolution of the satellite SSS product. Both original and filtered *in situ* data are finally stored in the MDB files.

Only for satellite L2 SSS data, a third step consist in filtering spurious data using the flags and associated recommendation as provided by the official data centers and described in 2.1.

2.4.2 *In situ*/Satellite Co-localization

In this step, each SSS satellite acquisition is co-localized with the filtered *in situ* measurements. The method used for co-localization differ if the satellite SSS is a swath product (so-called Level 2-types) or a time-space composite product (so-called Level 3/level 4-types).

- For L2 SSS swath data :

  If R_{sat} is the spatial resolution of the satellite swath SSS product, for each *in situ* data sample collected in the Pi-MEP database, the platform searches for all satellite SSS data found at grid nodes located within a radius of $R_{sat}/2$ from the *in situ* data location and

acquired with a time-lag from the *in situ* measurement date that is less or equal than ± 12 hours. If several satellite SSS samples are found to meet these criteria, the final satellite SSS match-up point is selected to be the closest in time from the *in situ* data measurement date. The final spatial and temporal lags between the *in situ* and satellite data are stored in the MDB files.

- For L3 and L4 composite SSS products :

  If R_{sat} is the spatial resolution of the composite satellite SSS product and D the period over which the composite product was built (e.g., periods of 1, 7, 8, 9, 10, 18 days, 1 month, etc..) with central time t_o, for each *in situ* data sample collected in the Pi-MEP database during period D, the platform searches for all satellite SSS data of the composite product found at grid nodes located within a radius of $R_{sat}/2$ from the *in situ* data location. If several satellite SSS product samples are found to meet these criteria, the final satellite SSS match-up point is chosen to be the composite SSS with central time t_o which is the closest in time from the *in situ* data measurement date. The final spatial and temporal lags between the *in situ* and satellite data are stored in the MDB files.

2.4.3 MDB pair Co-localization with auxiliary data and complementary information

MDB data consist of satellite and *in situ* SSS pairs but also of auxiliary geophysical parameters such as local and history of wind speed and rain rates, as well as various information (climatology, distance to coast, mixed layer depth, barrier layer thickness, etc) that can be derived from *in situ* data and which are included in the final match-up files. The collocation of auxiliary parameters and additional information is done for each *in situ* SSS measurement contained in the match-up files as follows :

If t_{insitu} is the time/date at which the *in situ* measurement is performed, we collect:

- The ASCAT wind speed product of the same day than t_{insitu} found at the ASCAT 1/4° grid node with closest distance from the *in situ* data location and the time series of the ASCAT wind speed at the same node for the 10 days prior the *in situ* measurement day.
- If the *in situ* data is located within the 60°N-60°S band, we select the CMORPH 3-hourly product the closest in time from t_{insitu} and found at the CMORPH 1/4° grid node with closest distance from the *in situ* data location. We then store the time series of the CMORPH rain rate at the same node for the 10 days prior the *in situ* measurement time.

For the given month/year of the *in situ* data, we select the ISAS and WOA fields for the same month (and same year for ISAS fields) and take the SSS analysis (monthly mean, std) found at the closest grid node from the *in situ* measurement.

The distance from the *in situ* SSS data location to the nearest coast is evaluated and provided in km. We use a distance-to-coast map at 1/4° resolution where small islands have been removed.

When vertical profiles of salinity (S) and temperature (T) are made available from the *in situ* measurements used to build the match-up (Argo or sea mammals), the following variables are included into each satellite/*in situ* match-up file:

1. The vertical distribution of pressure at which the profile were measured,
2. The vertical S(z) and T(z) profiles,
3. The vertical potential density anomaly profile $\sigma_0(z)$,

4. The Mixed Layer Depth (MLD). The MLD is defined here as the depth where the potential density has increased from the reference depth (10 meter) by a threshold equivalent to 0.2°C decrease in temperature at constant salinity: $\sigma_0 = \sigma_{010m} + \Delta\sigma_0$ with $\Delta\sigma_0 = \sigma_0(\theta_{10m} - 0.2, S_{10m}) - \sigma_0(\theta_{10m}, S_{10m})$ where θ_{10m} and S_{10m} are the temperature and salinity at the reference depth (i.e. 10 m) (de Boyer Montégut et al. (2004), de Boyer Montégut et al. (2007)).

5. The Top of the Thermocline Depth (TTD) is defined as the depth at which temperature decreases from its 10 m value by 0.2°C.

6. The Barrier Layer if present, is defined as the intermediate layer between the top of the thermocline and the bottom of the density mixed-layer and its thickness (BLT) is defined as the difference between the MLD and the TTD.

7. The vertical profile of the buoyancy frequency $N^2(z)$

The resulting match-ups files are serialized as NetCDF-4 files whose structure depends on the origin of the *in situ* data and is described in section 2.4.4.

2.4.4 Content of the Match-Up NetCDF files

```
netcdf pimep-mdb_aquarius-l3-jpl-v5-1m_tsg-legos-dm_20100116_v01 {
dimensions:
        TIME_SAT = UNLIMITED ; // (1 currently)
        TIME_TSG = 2190 ;
        N_DAYS_WIND = 10 ;
        N_3H_RAIN = 80 ;
        STRING25 = 25 ;
        STRING8 = 8 ;

    variables:
float DATE_TSG(TIME_TSG) ;
DATE_TSG:long_name = ”Date of TSG” ;
        DATE_TSG:units = ”days since 1990-01-01 00:00:00” ;
        DATE_TSG:standard_name = ”time” ;
        DATE_TSG:_FillValue = -999.f ;
float LATITUDE_TSG(TIME_TSG) ;
        LATITUDE_TSG:long_name = ”Latitude of TSG” ;
        LATITUDE_TSG:units = ”degrees_north” ;
        LATITUDE_TSG:valid_min = -90. ;
        LATITUDE_TSG:valid_max = 90. ;
        LATITUDE_TSG:standard_name = ”latitude” ;
        LATITUDE_TSG:_FillValue = -999.f ;
float LONGITUDE_TSG(TIME_TSG) ;
        LONGITUDE_TSG:long_name = ”Longitude of TSG” ;
        LONGITUDE_TSG:units = ”degrees_east” ;
        LONGITUDE_TSG:valid_min = -180. ;
        LONGITUDE_TSG:valid_max = 180. ;
        LONGITUDE_TSG:standard_name = ”longitude” ;
        LONGITUDE_TSG:_FillValue = -999.f ;
float SSS_TSG(TIME_TSG) ;
```

SSS_TSG:long_name = ”TSG SSS” ;
SSS_TSG:units = ”1” ;
SSS_TSG:salinity_scale = ”Practical Salinity Scale(PSS-78)” ;
SSS_TSG:standard_name = ”sea_water_salinity” ;
SSS_TSG:_FillValue = -999.f ;
float SST_TSG(TIME_TSG) ;
SST_TSG:long_name = ”TSG SST” ;
SST_TSG:units = ”degree Celsius” ;
SST_TSG:standard_name = ”sea_water_temperature” ;
SST_TSG:_FillValue = -999.f ;
float SSS_TSG_FILTERED(TIME_TSG) ;
SSS_TSG_FILTERED:long_name = ”TSG SSS median filtered at satellite spatial resolution” ;
SSS_TSG_FILTERED:units = ”1” ;
SSS_TSG_FILTERED:salinity_scale = ”Practical Salinity Scale(PSS-78)” ;
SSS_TSG_FILTERED:standard_name = ”sea_water_salinity” ;
SSS_TSG_FILTERED:_FillValue = -999.f ;
float SST_TSG_FILTERED(TIME_TSG) ;
SST_TSG_FILTERED:long_name = ”TSG SST median filtered at satellite spatial resolution” ;
SST_TSG_FILTERED:units = ”degree Celsius” ;
SST_TSG_FILTERED:standard_name = ”sea_water_temperature” ;
SST_TSG_FILTERED:_FillValue = -999.f ;
float DISTANCE_TO_COAST_TSG(TIME_TSG) ;
DISTANCE_TO_COAST_TSG:long_name = ”Distance to coasts at TSG location” ;
DISTANCE_TO_COAST_TSG:units = ”km” ;
DISTANCE_TO_COAST_TSG:_FillValue = -999.f ;
float PLATFORM_NUMBER_TSG(TIME_TSG) ;
PLATFORM_NUMBER_TSG:long_name = ”TSG unique identifier” ;
PLATFORM_NUMBER_TSG:conventions = ”WMO float identifier : A9IIIII” ;
PLATFORM_NUMBER_TSG:units = ”1” ;
PLATFORM_NUMBER_TSG:_FillValue = -999.f ;
float DATE_Satellite_product(TIME_Sat) ;
DATE_Satellite_product:long_name = ”Central time of satellite SSS file” ;
DATE_Satellite_product:units = ”days since 1990-01-01 00:00:00” ;
DATE_Satellite_product:standard_name = ”time” ;
float LATITUDE_Satellite_product(TIME_TSG) ;
LATITUDE_Satellite_product:long_name = ”Satellite product latitude at TSG location” ;
LATITUDE_Satellite_product:units = ”degrees_north” ;
LATITUDE_Satellite_product:valid_min = -90. ;
LATITUDE_Satellite_product:valid_max = 90. ;
LATITUDE_Satellite_product:standard_name = ”latitude” ;
LATITUDE_Satellite_product:_FillValue = -999.f ;
float LONGITUDE_Satellite_product(TIME_TSG) ;
LONGITUDE_Satellite_product:long_name = ”Satellite product longitude at TSG location” ;
LONGITUDE_Satellite_product:units = ”degrees_east” ;
LONGITUDE_Satellite_product:valid_min = -180. ;
LONGITUDE_Satellite_product:valid_max = 180. ;

LONGITUDE_Satellite_product:standard_name = ”longitude” ;
LONGITUDE_Satellite_product:_FillValue = -999.f ;
float SSS_Satellite_product(TIME_TSG) ;
SSS_Satellite_product:long_name = ”Satellite product SSS at TSG location” ;
SSS_Satellite_product:units = ”1” ;
SSS_Satellite_product:salinity_scale = ”Practical Salinity Scale(PSS-78)” ;
SSS_Satellite_product:standard_name = ”sea_surface_salinity” ;
SSS_Satellite_product:_FillValue = -999.f ;
float SST_Satellite_product(TIME_TSG) ;
SST_Satellite_product:long_name = ”Satellite product SST at TSG location” ;
SST_Satellite_product:units = ”degree Celsius” ;
SST_Satellite_product:standard_name = ”sea_surface_temperature” ;
SST_Satellite_product:_FillValue = -999.f ;
float Spatial_lags(TIME_TSG) ;
Spatial_lags:long_name = ”Spatial lag between TSG location and satellite SSS product pixel center” ;
Spatial_lags:units = ”km” ;
Spatial_lags:_FillValue = -999.f ;
float Time_lags(TIME_TSG) ;
Time_lags:long_name = ”Temporal lag between TSG time and satellite SSS product central time” ;
Time_lags:units = ”days” ;
Time_lags:_FillValue = -999.f ;
float ROSSBY_RADIUS_at_TSG(TIME_TSG) ;
ROSSBY_RADIUS_at_TSG:long_name = ”Baroclinic Rossby radius of deformation (Chelton et al., 1998) at TSG location” ;
ROSSBY_RADIUS_at_TSG:units = ”km” ;
ROSSBY_RADIUS_at_TSG:_FillValue = -999.f ;
float Ascat_daily_wind_at_TSG(TIME_TSG) ;
Ascat_daily_wind_at_TSG:long_name = ”Daily Ascat wind speed module at TSG location” ;
Ascat_daily_wind_at_TSG:units = ”m/s” ;
Ascat_daily_wind_at_TSG:_FillValue = -999.f ;
float CMORPH_3h_Rain_Rate_at_TSG(TIME_TSG) ;
CMORPH_3h_Rain_Rate_at_TSG:long_name = ”3-hourly CMORPH rain rate at TSG location” ;
CMORPH_3h_Rain_Rate_at_TSG:units = ”mm/3h” ;
CMORPH_3h_Rain_Rate_at_TSG:_FillValue = -999.f ;
float Ascat_10_prior_days_wind_at_TSG(TIME_TSG, N_DAYS_WIND) ;
Ascat_10_prior_days_wind_at_TSG:long_name = ”Prior 10 days time series of Ascat wind speed module at TSG location” ;
Ascat_10_prior_days_wind_at_TSG:units = ”m/s” ;
Ascat_10_prior_days_wind_at_TSG:_FillValue = -999.f ;
float CMORPH_10_prior_days_Rain_Rate_at_TSG(TIME_TSG, N_3H_RAIN) ;
CMORPH_10_prior_days_Rain_Rate_at_TSG:long_name = ”Prior 10 days times series of 3-hourly CMORPH Rain Rate at TSG location” ;
CMORPH_10_prior_days_Rain_Rate_at_TSG:units = ”mm/3h” ;
CMORPH_10_prior_days_Rain_Rate_at_TSG:_FillValue = -999.f ;
float SSS_ISAS_at_TSG(TIME_TSG) ;

SSS_ISAS_at_TSG:long_name = ”ISAS SSS (5m depth) at TSG location” ;
SSS_ISAS_at_TSG:units = ”1” ;
SSS_ISAS_at_TSG:salinity_scale = ”Practical Salinity Scale(PSS-78)” ;
SSS_ISAS_at_TSG:standard_name = ”sea_water_salinity” ;
SSS_ISAS_at_TSG:_FillValue = -999.f ;
float SSS_PCTVAR_ISAS_at_TSG(TIME_TSG) ;
SSS_PCTVAR_ISAS_at_TSG:long_name = ”Error on ISAS SSS (5m depth) at TSG location (% variance)” ;
SSS_PCTVAR_ISAS_at_TSG:units = ”%” ;
SSS_PCTVAR_ISAS_at_TSG:_FillValue = -999.f ;
float SSS_WOA13_at_TSG(TIME_TSG) ;
SSS_WOA13_at_TSG:long_name = ”WOA 2013 (DECAV-1deg) SSS (0m depth) at TSG location” ;
SSS_WOA13_at_TSG:units = ”1” ;
SSS_WOA13_at_TSG:salinity_scale = ”Practical Salinity Scale(PSS-78)” ;
SSS_WOA13_at_TSG:standard_name = ”sea_surface_salinity” ;
SSS_WOA13_at_TSG:_FillValue = -999.f ;
float SSS_STD_WOA13_at_TSG(TIME_TSG) ;
SSS_STD_WOA13_at_TSG:long_name = ”WOA 2013 (DECAV-1deg) SSS STD (0m depth) at TSG location ” ;
SSS_STD_WOA13_at_TSG:units = ”1” ;
SSS_STD_WOA13_at_TSG:_FillValue = -999.f ;
float SSS_ISAS15_at_TSG(N_prof) ;
SSS_ISAS15_at_TSG:long_name = ”Monthly ISAS-15 SSS (5m depth) at TSG location” ;
SSS_ISAS15_at_TSG:units = ”1” ;
SSS_ISAS15_at_TSG:salinity_scale = ”Practical Salinity Scale (PSS-78)” ;
SSS_ISAS15_at_TSG:standard_name = ”sea_water_salinity” ;
SSS_ISAS15_at_TSG:_FillValue = -999.f ;
float SSS_PCTVAR_ISAS15_at_TSG(N_prof) ;
SSS_PCTVAR_ISAS15_at_TSG:long_name = ”Error on monthly ISAS-15 SSS (5m depth) at TSG location (% variance)” ;
SSS_PCTVAR_ISAS15_at_TSG:units = ”%” ;
SSS_PCTVAR_ISAS15_at_TSG:_FillValue = -999.f ;
float SSS_WOA18_at_TSG(N_prof) ;
SSS_WOA18_at_TSG:long_name = ”Monthly WOA 2018 (DECAV-1deg) SSS (0m depth) at TSG location” ;
SSS_WOA18_at_TSG:units = ”1” ;
SSS_WOA18_at_TSG:salinity_scale = ”Practical Salinity Scale (PSS-78)” ;
SSS_WOA18_at_TSG:standard_name = ”sea_surface_salinity” ;
SSS_WOA18_at_TSG:_FillValue = -999.f ;
float SSS_STD_WOA18_at_TSG(N_prof) ;
SSS_STD_WOA18_at_TSG:long_name = ”Monthly WOA 2018 (DECAV-1deg) SSS STD (0m depth) at TSG location ” ;
SSS_STD_WOA18_at_TSG:units = ”1” ;
SSS_STD_WOA18_at_TSG:_FillValue = -999.f ;
float SEA_ICE_CONCENTRATION_at_TSG(N_prof) ;
SEA_ICE_CONCENTRATION_at_TSG:long_name = ”Daily sea ice area fraction (EUMETSAT OSI-SAF OSI-450) at TSG location (%)” ;
SEA_ICE_CONCENTRATION_at_TSG:units = ”1” ;

SEA_ICE_CONCENTRATION_at_TSG:standard_name = ”sea_ice_area_fraction” ;
SEA_ICE_CONCENTRATION_at_TSG:_FillValue = -999.f ;
float CCMP_6h_Wind_Speed_at_TSG(N_prof) ;
CCMP_6h_Wind_Speed_at_TSG:long_name = ”6-hourly CCMP wind speed at TSG location” ;
CCMP_6h_Wind_Speed_at_TSG:units = ”m s-1” ;
CCMP_6h_Wind_Speed_at_TSG:standard_name = ”wind_speed” ;
CCMP_6h_Wind_Speed_at_TSG:_FillValue = -999.f ;
float CCMP_10_prior_days_Wind_Speed_at_TSG(N_prof, N_DAYS_WIND_CCMP) ;
CCMP_10_prior_days_Wind_Speed_at_TSG:long_name = ”Prior 10 days time series of CCMP wind speed at TSG location” ;
CCMP_10_prior_days_Wind_Speed_at_TSG:units = ”m s-1” ;
CCMP_10_prior_days_Wind_Speed_at_TSG:standard_name = ”wind_speed” ;
CCMP_10_prior_days_Wind_Speed_at_TSG:_FillValue = -999.f ;
float CDM_GLOBCOLOUR_at_TSG(N_prof) ;
CDM_GLOBCOLOUR_at_TSG:long_name = ”8-day Coloured dissolved and detrital organic materials - mean of the binned pixels at TSG location” ;
CDM_GLOBCOLOUR_at_TSG:units = ”m-1” ;
CDM_GLOBCOLOUR_at_TSG:standard_name = ”volume_absorption_coefficient_of_radiative_flux_in_sea_water_
;
CDM_GLOBCOLOUR_at_TSG:_FillValue = -999.f ;
float CHL1_GLOBCOLOUR_at_TSG(N_prof) ;
CHL1_GLOBCOLOUR_at_TSG:long_name = ”8-day Chlorophyll concentration - mean of the binned pixels at TSG location” ;
CHL1_GLOBCOLOUR_at_TSG:units = ”mg m-3” ;
CHL1_GLOBCOLOUR_at_TSG:standard_name = ”mass_concentration_of_chlorophyll_a_in_sea_water”
;
CHL1_GLOBCOLOUR_at_TSG:_FillValue = -999.f ;
float EVAPORATION_OAFLUX_at_TSG(N_prof) ;
EVAPORATION_OAFLUX_at_TSG:long_name = ”Daily mean evaporation rate (OAFlux) at TSG location” ;
EVAPORATION_OAFLUX_at_TSG:units = ”cm year-1” ;
EVAPORATION_OAFLUX_at_TSG:_FillValue = -999.f ;
float SSS_SCRIPPS_at_TSG(N_prof) ;
SSS_SCRIPPS_at_TSG:long_name = ”Argo gridded monthly mean SSS (0m depth) from SCRIPPS (Roemmich-Gilson) at TSG location” ;
SSS_SCRIPPS_at_TSG:units = ”1” ;
SSS_SCRIPPS_at_TSG:salinity_scale = ”Practical Salinity Scale (PSS-78)” ;
SSS_SCRIPPS_at_TSG:standard_name = ”sea_water_salinity” ;
SSS_SCRIPPS_at_TSG:_FillValue = -999.f ;
float SSS_IPRC_at_TSG(N_prof) ;
SSS_IPRC_at_TSG:long_name = ”Argo gridded monthly mean SSS (0m depth) from IPRC at TSG location” ;
SSS_IPRC_at_TSG:units = ”1” ;
SSS_IPRC_at_TSG:salinity_scale = ”Practical Salinity Scale (PSS-78)” ;
SSS_IPRC_at_TSG:standard_name = ”sea_water_salinity” ;
SSS_IPRC_at_TSG:_FillValue = -999.f ;
float SST_AVHRR_at_TSG(N_prof) ;
SST_AVHRR_at_TSG:long_name = ”Daily OI AVHRR-only v2 SST (Reynolds et al., 2007)

at TSG location" ;
SST_AVHRR_at_TSG:units = "degree Celsius" ;
SST_AVHRR_at_TSG:standard_name = "sea_water_temperature" ;
SST_AVHRR_at_TSG:_FillValue = -999.f ;
float U_EKMAN_GLOBCURRENT_at_TSG(N_prof) ;
U_EKMAN_GLOBCURRENT_at_TSG:long_name = "15m depth Ekman current velocity: zonal component at TSG location" ;
U_EKMAN_GLOBCURRENT_at_TSG:units = "m s-1" ;
U_EKMAN_GLOBCURRENT_at_TSG:_FillValue = -999.f ;
float V_EKMAN_GLOBCURRENT_at_TSG(N_prof) ;
V_EKMAN_GLOBCURRENT_at_TSG:long_name = "15m depth Ekman current velocity: meridian component at TSG location" ;
V_EKMAN_GLOBCURRENT_at_TSG:units = "m s-1" ;
V_EKMAN_GLOBCURRENT_at_TSG:_FillValue = -999.f ;
float U_GEOSTROPHIC_GLOBCURRENT_at_TSG(N_prof) ;
U_GEOSTROPHIC_GLOBCURRENT_at_TSG:long_name = "Absolute geostrophic velocity: zonal component at TSG location" ;
U_GEOSTROPHIC_GLOBCURRENT_at_TSG:units = "m s-1" ;
U_GEOSTROPHIC_GLOBCURRENT_at_TSG:_FillValue = -999.f ;
float V_GEOSTROPHIC_GLOBCURRENT_at_TSG(N_prof) ;
V_GEOSTROPHIC_GLOBCURRENT_at_TSG:long_name = "Absolute geostrophic velocity: meridian component at TSG location" ;
V_GEOSTROPHIC_GLOBCURRENT_at_TSG:units = "m s-1" ;
V_GEOSTROPHIC_GLOBCURRENT_at_TSG:_FillValue = -999.f ;

// global attributes:
:Conventions = "CF-1.6" ;
:title = "TSG-LEGOS-DM Match-Up Database" ;
:Satellite_product_name = "Aquarius-L3-JPL-V5-MONTHLY" ;
:Satellite_product_spatial_resolution = "1 deg" ;
:Satellite_product_temporal_resolution = "Monthly" ;
:Satellite_product_filename = " v5/monthly/2011/sss201109.v5.0cap.nc" ;
:Match-Up_spatial_window_radius_in_km = 55;
:Match-Up_temporal_window_radius_in_days = 15;
:start_time = "20100114T000005Z" ;
:stop_time = "20100118T235026Z" ;
:northernmost_latitude = 77.676f ;
:sourthenmost_latitude = -66.423f ;
:westernmost_longitude = -179.219f ;
:easternmost_longitude = 179.199f ;
:geospatial_lat_units = "degrees north" ;
:geospatial_lat_resolution = "1 deg" ;
:geospatial_lon_units = "degrees east" ;
:geospatial_lon_resolution = "1 deg" ;
:institution = "ESA-IFREMER-ODL-OCEANSCOPE" ;
:project_name = "SMOS Pilot-Mission Exploitation Platform (Pi-MEP) for salinity" ;
:project_url = "https://www.salinity-pimep.org" ;
:license = "Pi-MEP data use is free and open" ;
:product_version = "1.0" ;

:keywords = "Oceans > Ocean Salinity > Sea Surface Salinity" ;
:acknowledgment = "Please acknowledge the use of these data with the following statement: These data were provided by the SMOS Pilot-Mission Exploitation Platform (Pi-MEP) for salinity" ;
:source = " v5/monthly/2011/sss201109.v5.0cap.nc" ;
:references = "https://www.salinity-pimep.org" ;
:history = "Processed on 2018-04-18 using MDB_generator" ;
:date_created = "2018-04-18 17:09:30" ;
}

2.5 MDB characteristics for the particular *in situ*/satellite pairs

2.5.1 Number of paired SSS data as a function of time and distance to coast

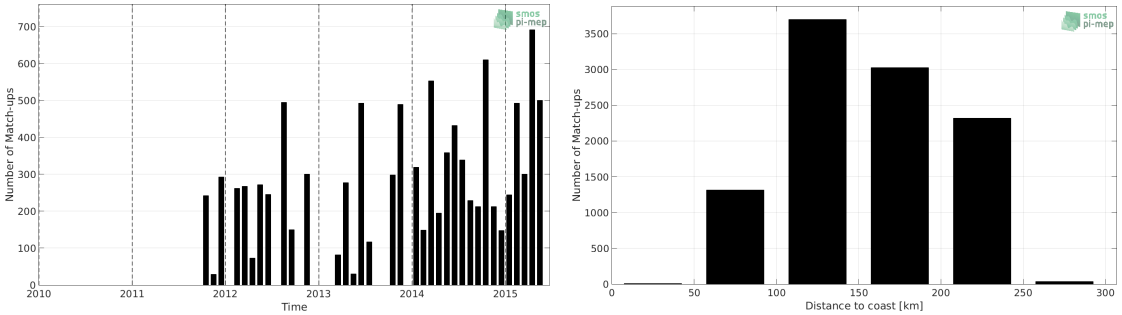

(a) (b)

Figure 1: Number of match-ups between TSG-LEGOS-DM and Aquarius-L3-JPL-V5-MONTHLY SSS as a function of time (a) and as function of the distance to coast (b) over the Sea of Japan Pi-MEP region and for the full satellite product period.

2.5.2 Histograms of the SSS match-ups

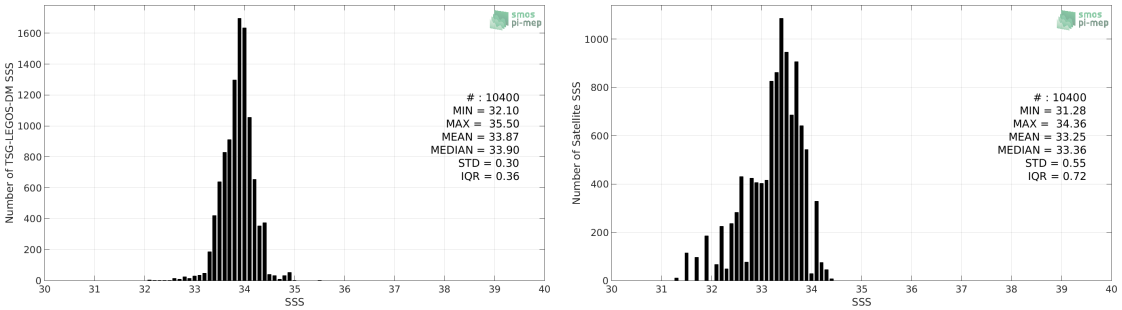

(a) (b)

Figure 2: Histograms of SSS from TSG-LEGOS-DM (a) and Aquarius-L3-JPL-V5-MONTHLY (b) considering all match-up pairs per bins of 0.1 over the Sea of Japan Pi-MEP region and for the full satellite product period.

2.5.3 Distribution of *in situ* SSS depth measurements

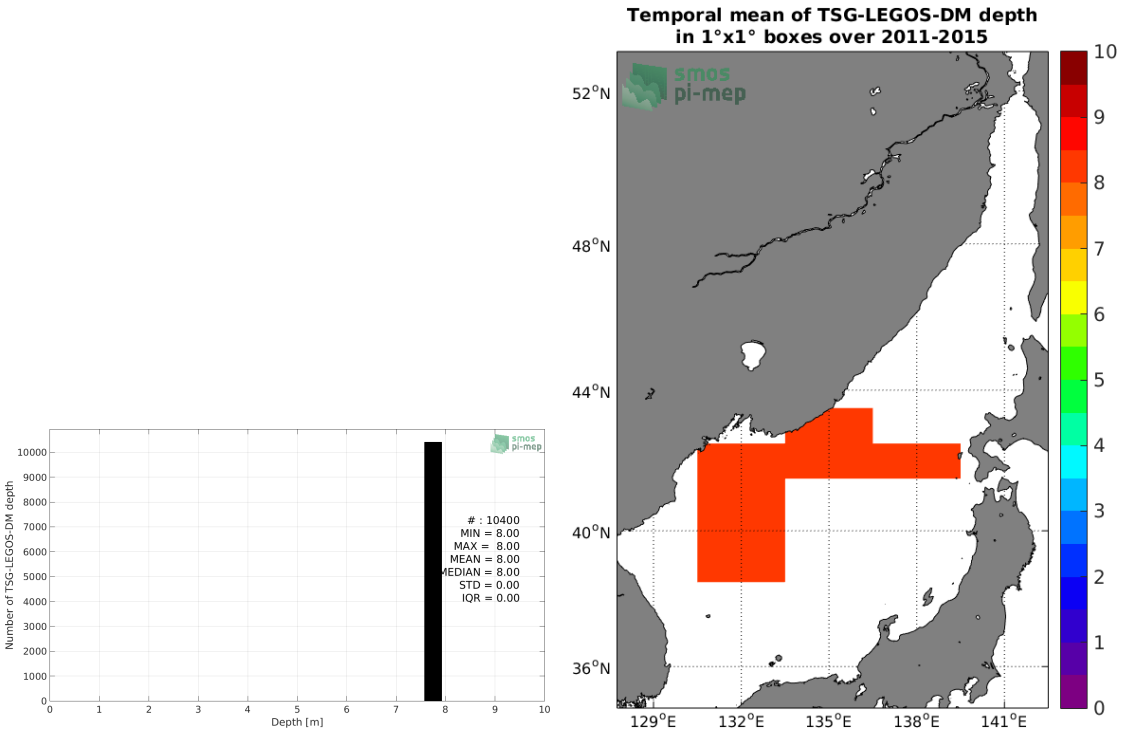

(a) (b)

Figure 3: Histograms of the depth of the upper level SSS measurements from TSG-LEGOS-DM in the Match-up DataBase for the Sea of Japan Pi-MEP region (a) and temporal mean spatial distribution of pressure of the *in situ* SSS data over 1°x1° boxes and for the full satellite product period (b).

2.5.4 Spatial Distribution of Match-ups

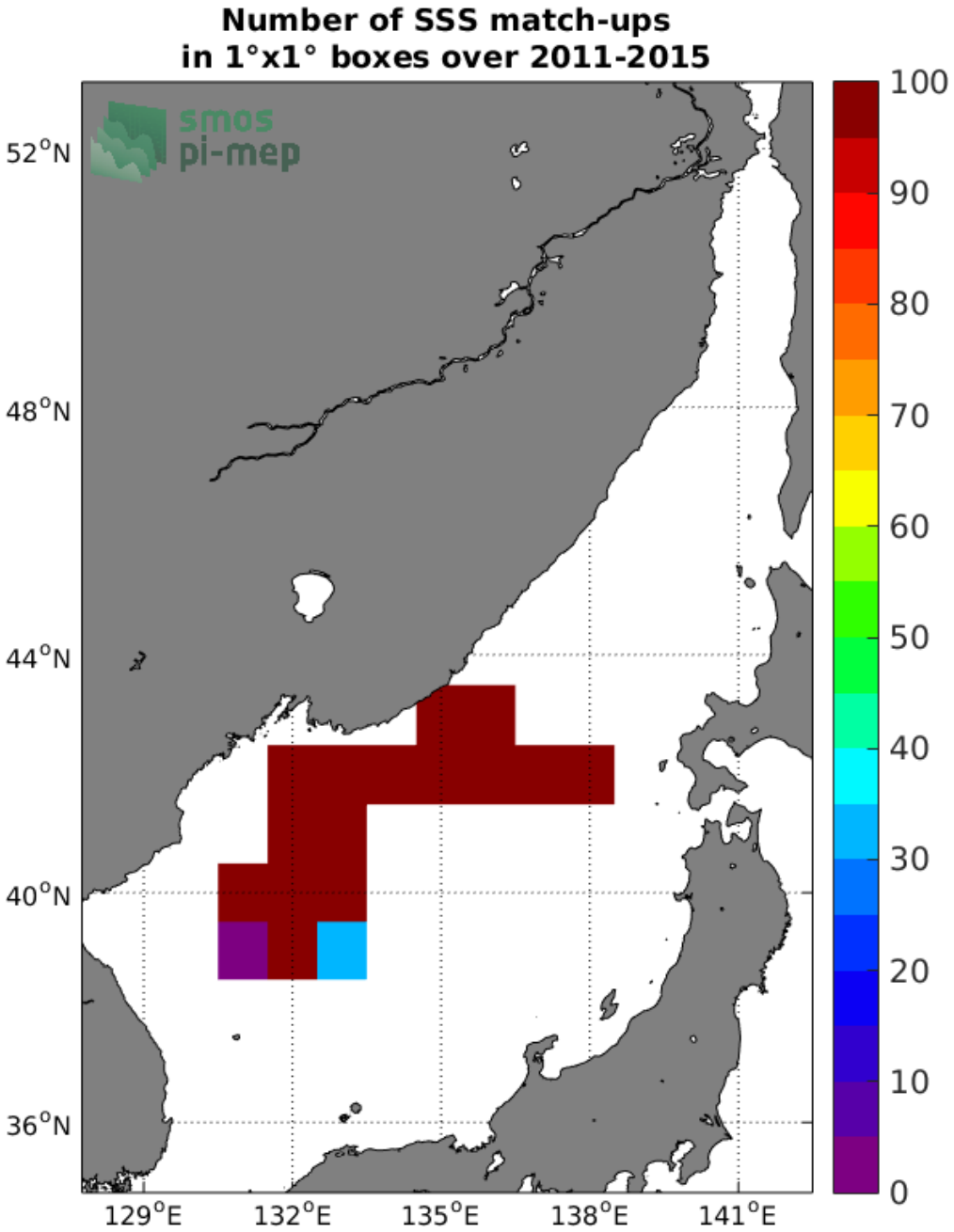

Figure 4: Number of SSS match-ups between TSG-LEGOS-DM SSS and the Aquarius-L3-JPL-V5-MONTHLY SSS product for the Sea of Japan Pi-MEP region over 1°x1° boxes and for the full satellite product period.

2.5.5 Histograms of the spatial and temporal lags of the match-ups pairs

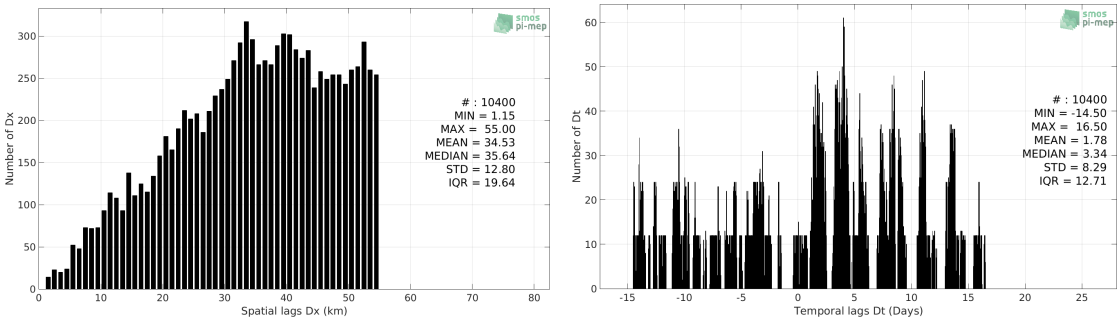

(a) (b)

Figure 5: Histograms of the spatial (a) and temporal (b) lags between the time of the TSG-LEGOS-DM measurements and the date of the corresponding Aquarius-L3-JPL-V5-MONTHLY SSS product.

3 MDB file Analyses

3.1 Spatial Maps of the Temporal mean and Std of *in situ* and satellite SSS and of the difference (ΔSSS)

In Figure 6, we show maps of temporal mean (left) and standard deviation (right) of the Aquarius-L3-JPL-V5-MONTHLY (top) and of the TSG-LEGOS-DM *in situ* dataset at the collected Pi-MEP match-up pairs. The temporal mean and std are gridded over the full satellite product period and over spatial boxes of size 1°x1°.

At the bottom of Figure 6, the temporal mean (left) and standard deviation (right) of the differences between the satellite SSS product and *in situ* data found at match-up pairs, namely ΔSSS(Satellite -TSG-LEGOS-DM), is also gridded over the full satellite product period and over spatial boxes of size 1°x1°.

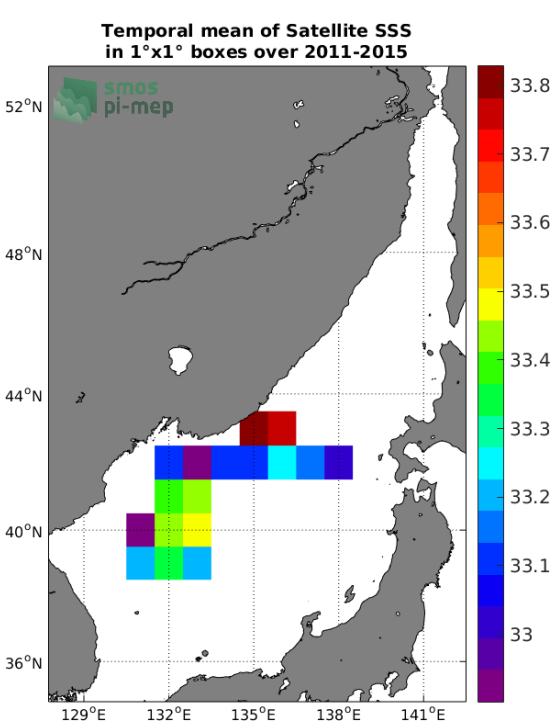

(a) MEAN(Satellite SSS)

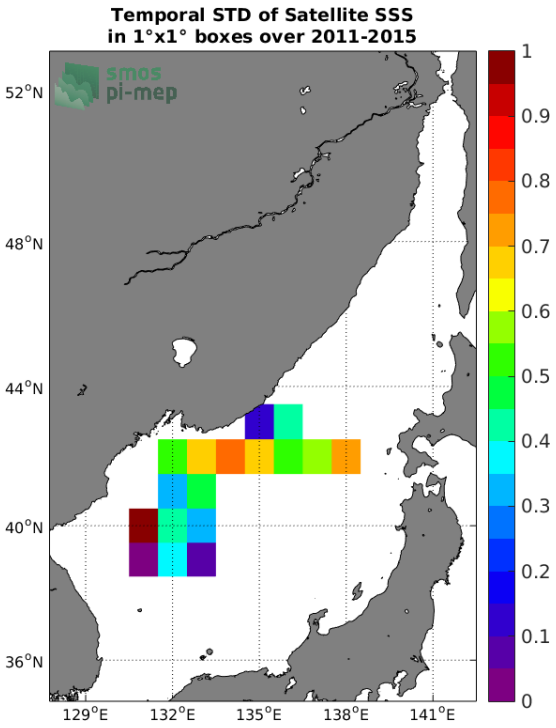

(b) Std(Satellite SSS)

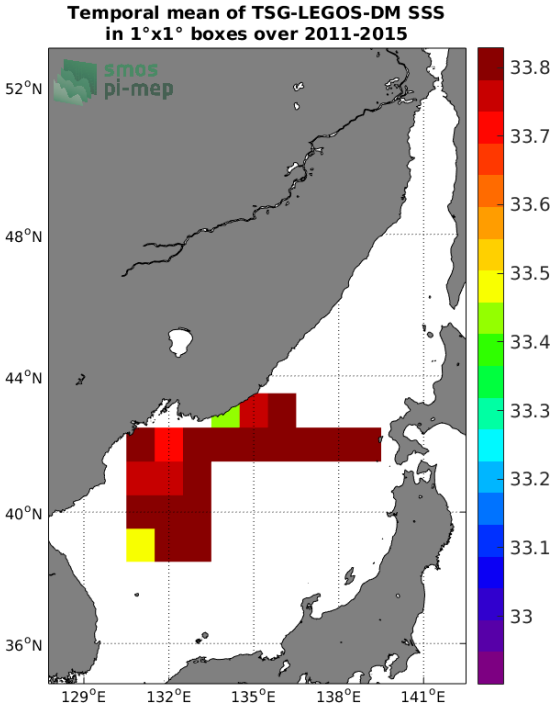

(c) MEAN(TSG-LEGOS-DM SSS)

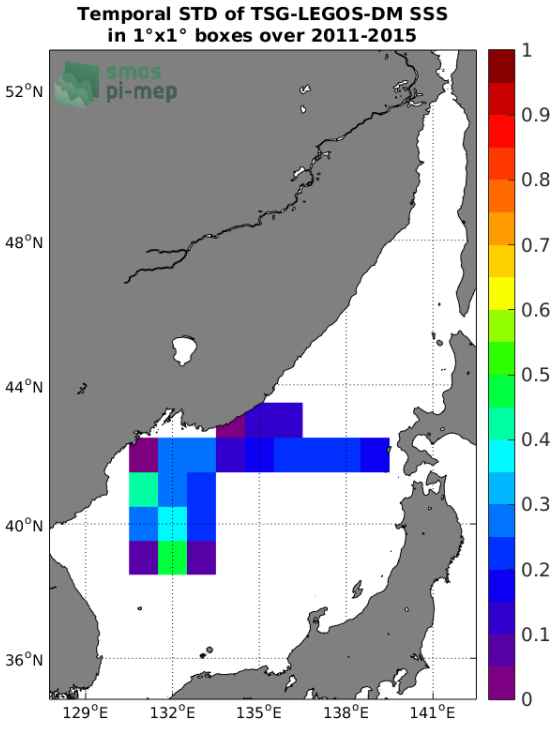

(d) Std(TSG-LEGOS-DM SSS)

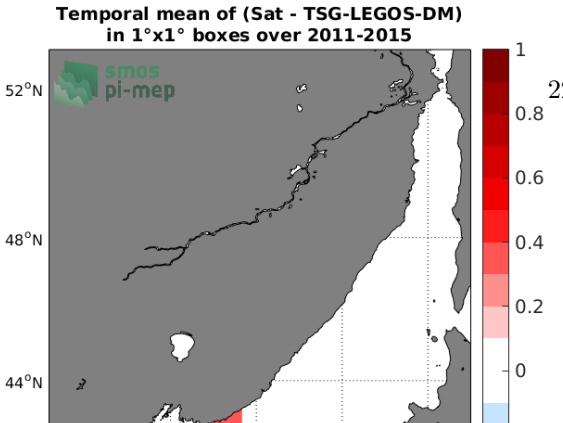

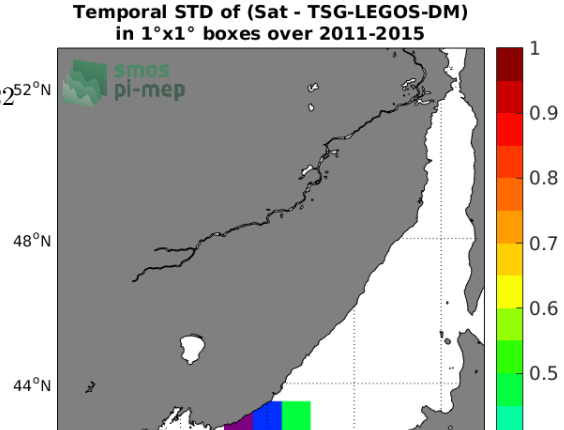

3.2 Time series of the monthly median and Std of *in situ* and satellite SSS and of the (ΔSSS)

In the top panel of Figure 7, we show the time series of the monthly median SSS estimated over the full Sea of Japan Pi-MEP region for both Aquarius-L3-JPL-V5-MONTHLY satellite SSS product (in black) and the TSG-LEGOS-DM *in situ* dataset (in blue) at the collected Pi-MEP match-up pairs.

In the middle panel of Figure 7, we show the time series of the monthly median of ΔSSS (Satellite - TSG-LEGOS-DM) for the collected Pi-MEP match-up pairs and estimated over the full Sea of Japan Pi-MEP region.

In the bottom panel of Figure 7, we show the time series of the monthly standard deviation of the ΔSSS (Satellite - TSG-LEGOS-DM) for the collected Pi-MEP match-up pairs and estimated over the full Sea of Japan Pi-MEP region.

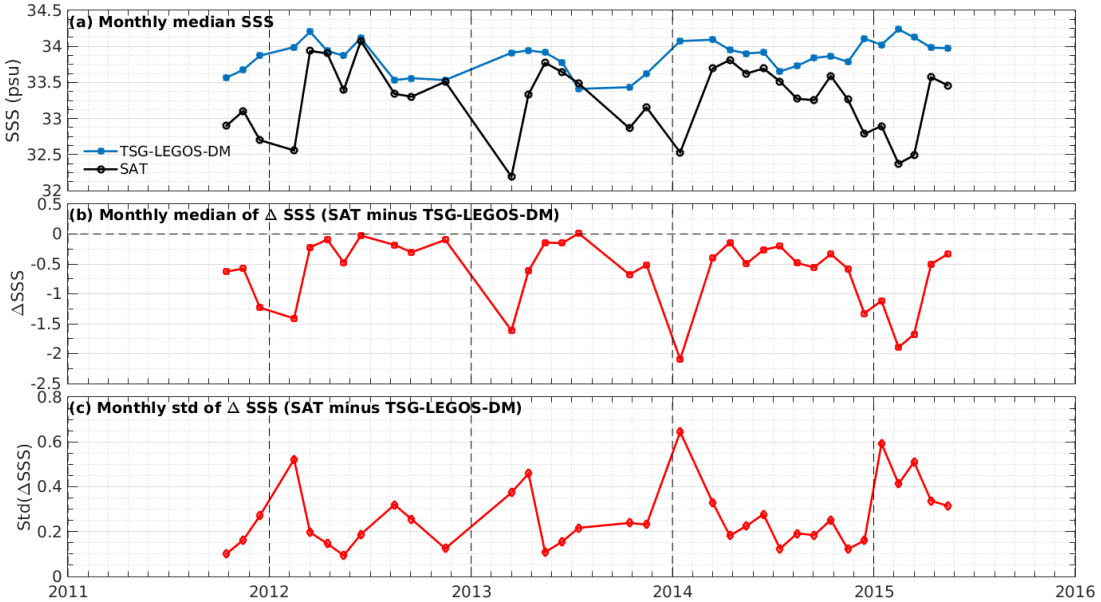

Figure 7: Time series of the monthly median SSS (top), median of ΔSSS (Satellite - TSG-LEGOS-DM) and Std of ΔSSS (Satellite - TSG-LEGOS-DM) over the Sea of Japan Pi-MEP region considering all match-ups collected by the Pi-MEP.

3.3 Zonal mean and Std of *in situ* and satellite SSS and of the ΔSSS

In Figure 8 left panel, we show the zonal mean SSS considering all Pi-MEP match-up pairs for both Aquarius-L3-JPL-V5-MONTHLY satellite SSS product (in black) and the TSG-LEGOS-DM *in situ* dataset (in blue). The full satellite SSS product period is used to derive the mean.

In the right panel of Figure 8, we show the zonal mean of ΔSSS (Satellite - TSG-LEGOS-DM) for all the collected Pi-MEP match-up pairs estimated over the full satellite product period.

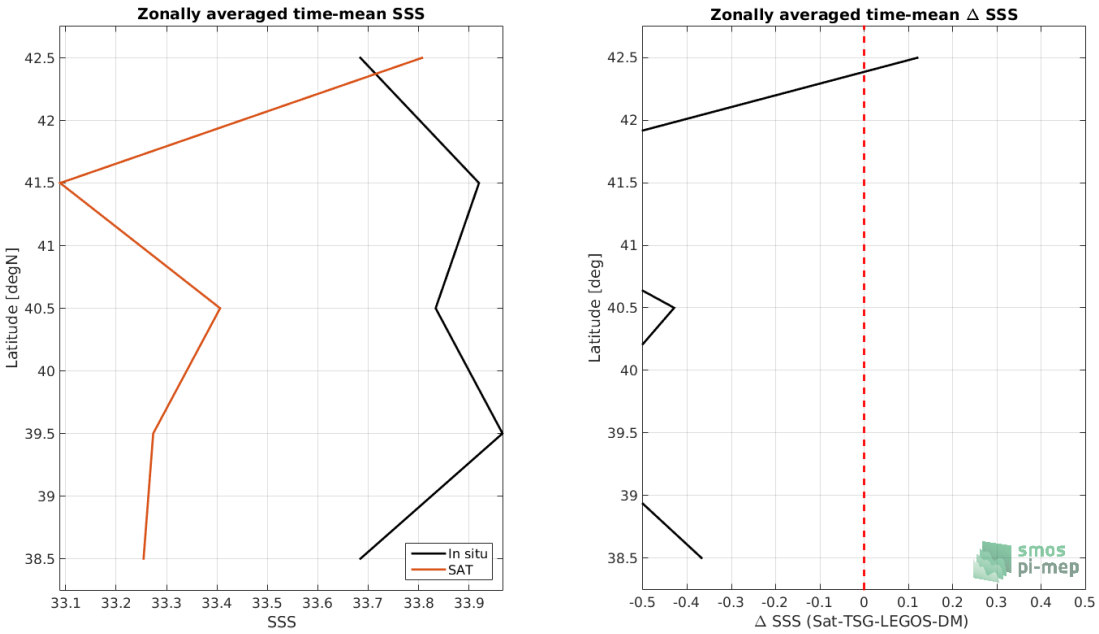

Figure 8: Left panel: Zonal mean SSS from Aquarius-L3-JPL-V5-MONTHLY satellite product (black) and from TSG-LEGOS-DM (blue). Right panel: Zonal mean of ΔSSS (Satellite - TSG-LEGOS-DM) for all the collected Pi-MEP match-up pairs estimated over the full satellite product period.

3.4 Scatterplots of satellite vs *in situ* SSS by latitudinal bands

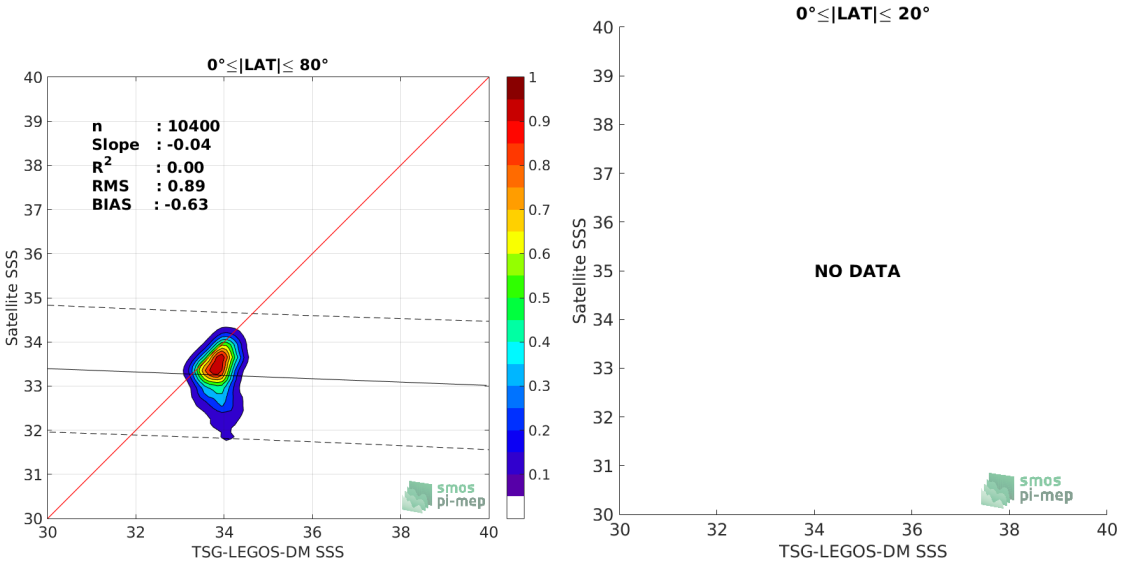

(a) $0° \leq |\text{LAT}| \leq 80°$

(b) $0° \leq |\text{LAT}| \leq 20°$

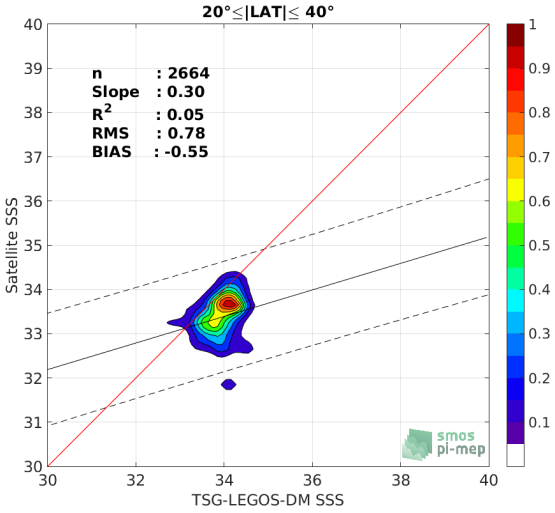

(c) $20° \leq |\text{LAT}| \leq 40°$

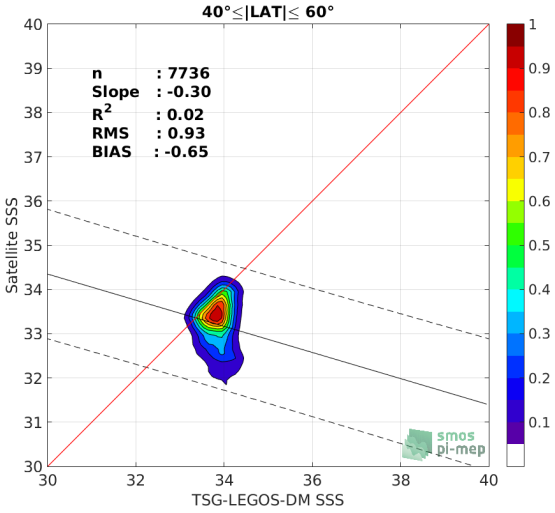

(d) $40° \leq |\text{LAT}| \leq 60°$

Figure 9: Contour maps of the concentration of Aquarius-L3-JPL-V5-MONTHLY SSS (y-axis) versus TSG-LEGOS-DM SSS (x-axis) at match-up pairs for different latitude bands. For each plot, the red line shows x=y. The black thin and dashed lines indicate a linear fit through the data cloud and the ±95% confidence levels, respectively. The number match-up pairs n, the slope and R^2 coefficient of the linear fit, the root mean square (RMS) and the mean bias between satellite and *in situ* data are indicated for each latitude band in each plots.

3.5 Time series of the monthly median and Std of the ΔSSS sorted by latitudinal bands

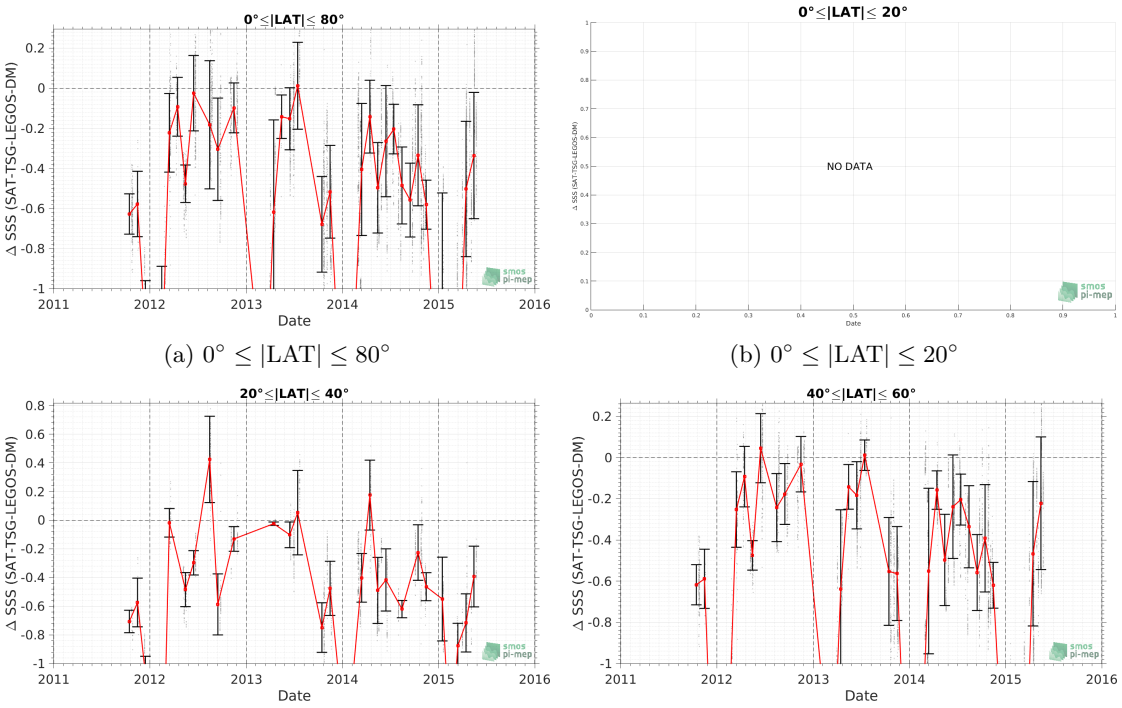

(a) $0° \leq |\text{LAT}| \leq 80°$

(b) $0° \leq |\text{LAT}| \leq 20°$

(c) $20° \leq |\text{LAT}| \leq 40°$

(d) $40° \leq |\text{LAT}| \leq 60°$

Figure 10: Monthly median (red curves) of ΔSSS (Satellite - TSG-LEGOS-DM) and ±1 Std (black vertical thick bars) as function of time for all the collected Pi-MEP match-up pairs estimated over the Sea of Japan Pi-MEP region and for the full satellite product period are shown for different latitude bands: (a) 80°S-80°N, (b) 20°S-20°N, (c) 40°S-20°S and 20°N-40°N and (d) 60°S-40°S and 40°N-60°N.

3.6 ΔSSS sorted as function of geophysical parameters

In Figure 11, we classify the match-up differences ΔSSS (Satellite - *in situ*) between Aquarius-L3-JPL-V5-MONTHLY and TSG-LEGOS-DM SSS as function of the geophysical conditions at match-up points. The mean and std of ΔSSS (Satellite - TSG-LEGOS-DM) is thus evaluated as function of the

- *in situ* SSS values per bins of width 0.2,
- *in situ* SST values per bins of width 1°C,
- ASCAT daily wind values per bins of width 1 m/s,
- CMORPH 3-hourly rain rates per bins of width 1 mm/h, and,
- distance to coasts per bins of width 50 km.

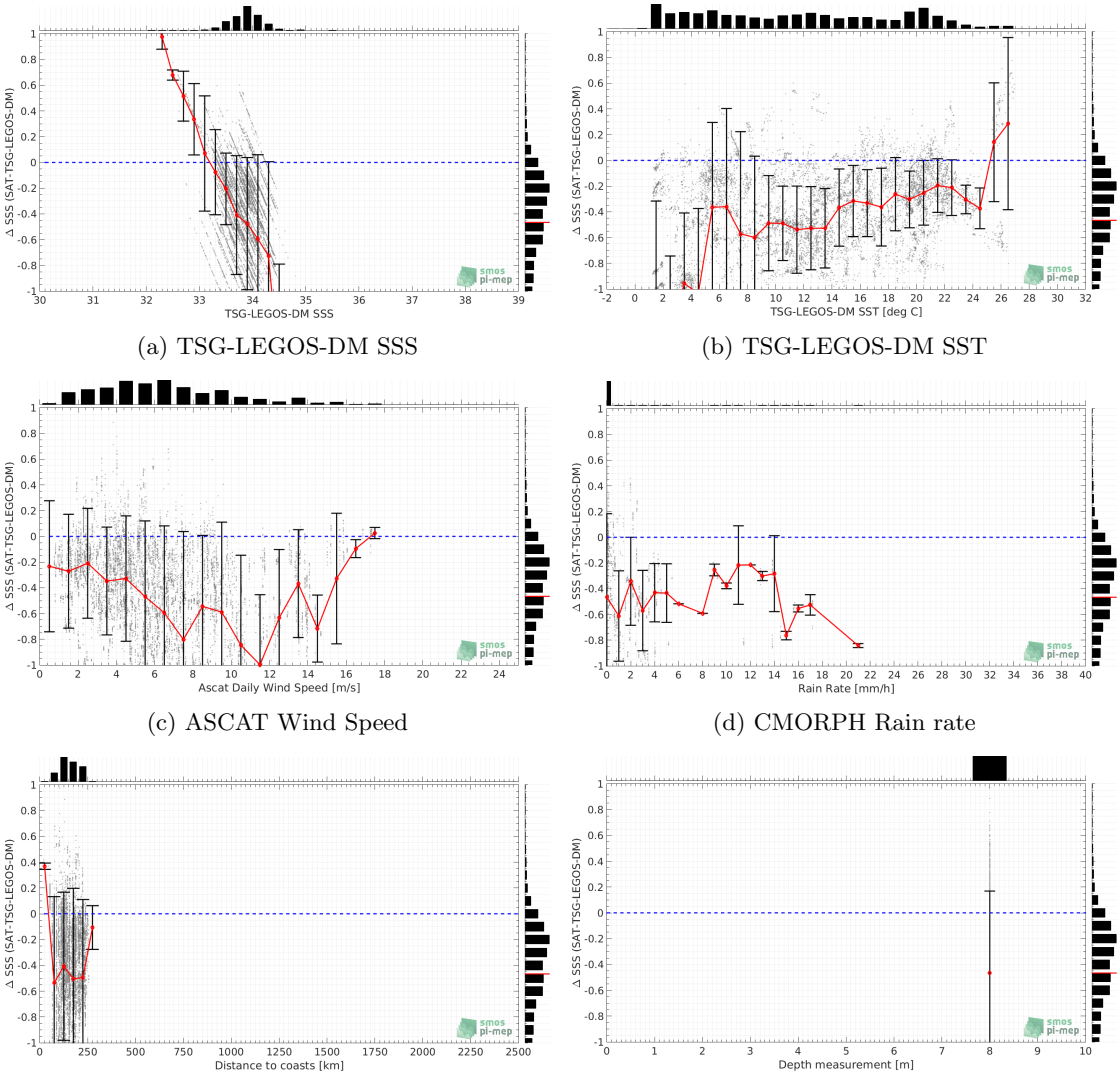

(a) TSG-LEGOS-DM SSS

(b) TSG-LEGOS-DM SST

(c) ASCAT Wind Speed

(d) CMORPH Rain rate

(e) Distance to coast

(f) *In situ* measurement Depth

Figure 11: ΔSSS (Satellite - TSG-LEGOS-DM) sorted as function of TSG-LEGOS-DM SSS values a), TSG-LEGOS-DM SST b), ASCAT Wind speed c), CMORPH rain rate d), distance to coast (e) and *in situ* measurement depth (f). In all plots the median and Std of ΔSSS for each bin is indicated by the red curves and black vertical thick bars (±1 Std)

3.7 ΔSSS maps and statistics for different geophysical conditions

In Figures 12 and 13, we focus on sub-datasets of the match-up differences ΔSSS (Satellite - *in situ*) between Aquarius-L3-JPL-V5-MONTHLY and TSG-LEGOS-DM for the following specific geophysical conditions:

- **C1**:if the local value at *in situ* location of estimated rain rate is zero, mean daily wind is in the range [3, 12] m/s, the SST is $> 5°C$ and distance to coast is > 800 km.
- **C2**:if the local value at *in situ* location of estimated rain rate is zero, mean daily wind is

in the range [3, 12] m/s.

- **C3**:if the local value at *in situ* location of estimated rain rate is high (ie. > 1 mm/h) and mean daily wind is low (ie. < 4 m/s).
- **C5**:if the *in situ* data is located where the climatological SSS standard deviation is low (ie. above < 0.2).
- **C6**:if the *in situ* data is located where the climatological SSS standard deviation is high (ie. above > 0.2).

For each of these conditions, the temporal mean (gridded over spatial boxes of size 1°x1°) and the histogram of the difference ΔSSS (Satellite - *in situ*) are presented.

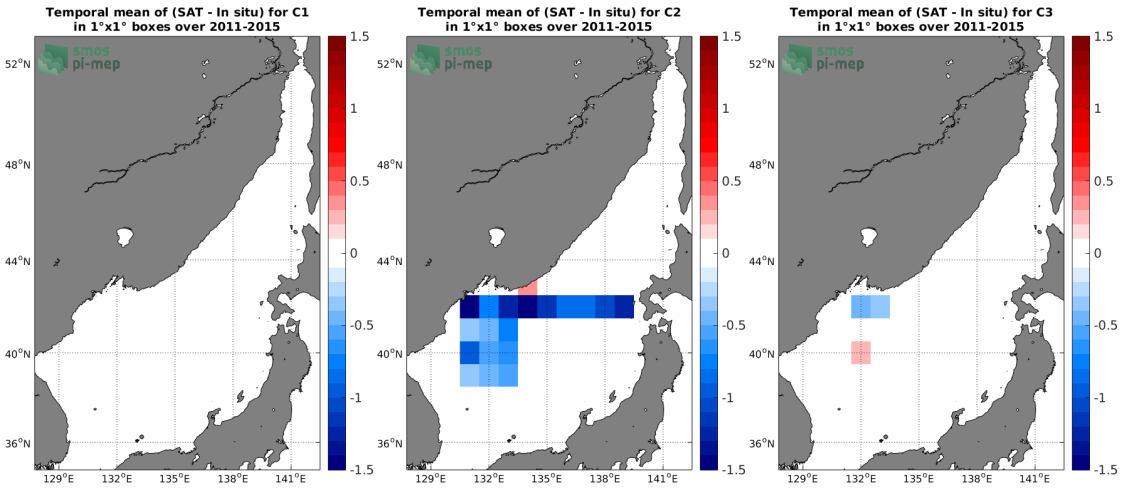

(a) RR=0 mm/h, 3< U_{10} <12 m/s, SST>5°C, distance to coast > 800 km (b) RR=0 mm/h, 3< U_{10} <12 m/s (c) RR>1mm/h and U_{10} <4m/s

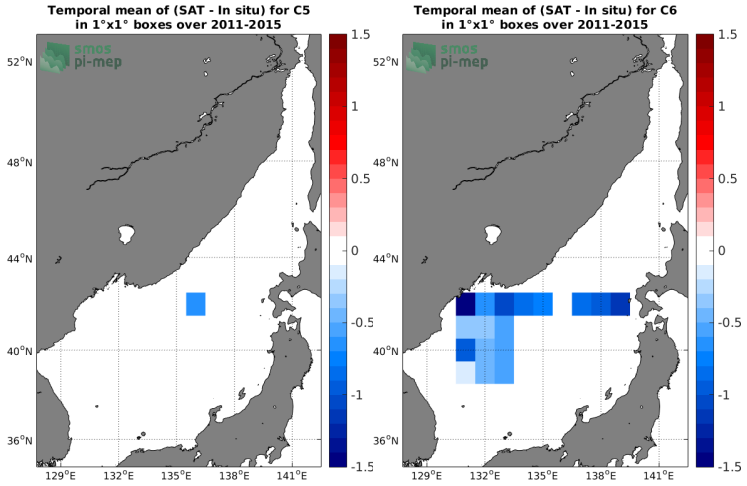

(d) WOA2013 SSS Std<0.2 (e) WOA2013 SSS Std>0.2

Figure 12: Temporal mean gridded over spatial boxes of size 1°x1° of ΔSSS (Aquarius-L3-JPL-V5-MONTHLY - TSG-LEGOS-DM) for 5 different subdatasets corresponding to:RR=0 mm/h, 3< U_{10} <12 m/s, SST>5°C, distance to coast > 800 km (a), RR=0 mm/h, 3< U_{10} <12 m/s (b), RR>1mm/h and U_{10} <4m/s (c), WOA2013 SSS Std<0.2 (d), WOA2013 SSS Std>0.2 (e).

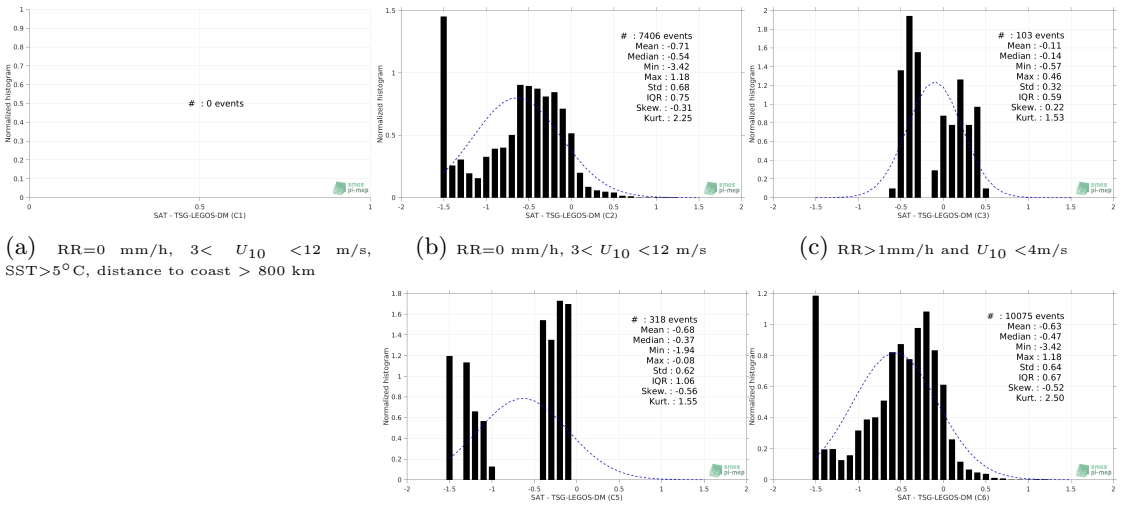

(a) RR=0 mm/h, 3< U_{10} <12 m/s, SST>5°C, distance to coast > 800 km (b) RR=0 mm/h, 3< U_{10} <12 m/s (c) RR>1mm/h and U_{10} <4m/s

(d) WOA2013 SSS Std<0.2 (e) WOA2013 SSS Std>0.2

Figure 13: Normalized histogram of ΔSSS (Aquarius-L3-JPL-V5-MONTHLY - TSG-LEGOS-DM) for 5 different subdatasets corresponding to: RR=0 mm/h, 3< U_{10} <12 m/s, SST>5°C, distance to coast > 800 km (a), RR=0 mm/h, 3< U_{10} <12 m/s (b), RR>1mm/h and U_{10} <4m/s (c), WOA2013 SSS Std<0.2 (d), WOA2013 SSS Std>0.2 (e).

4 Summary

► Table 1 shows the mean, median, standard deviation (Std), root mean square (RMS), interquartile range (IQR), correlation coefficient (r^2) and robust standard deviation (Std*) of the match-up differences ΔSSS (Satellite - *in situ*) between Aquarius-L3-JPL-V5-MONTHLY and TSG-LEGOS-DM derived over the Sea of Japan Pi-MEP region and for the full satellite product period and for the following conditions:

- all: All the match-up pairs satellite/*in situ* SSS values are used to derive the statistics
- C1: only pairs where RR=0 mm/h, 3< U_{10} <12 m/s, SST>5°C, distance to coast > 800 km
- C2: only pairs where RR=0 mm/h, 3< U_{10} <12 m/s
- C3: only pairs where RR>1mm/h and U_{10} <4m/s
- C5: only pairs where WOA2013 SSS Std<0.2
- C6: only pairs at WOA2013 SSS Std>0.2
- C7a: only pairs with a distance to coast < 150 km.
- C7b: only pairs with a distance to coast in the range [150, 800] km.
- C7c: only pairs with a distance to coast > 800 km.
- C8a: only pairs where SST is < 5°C.
- C8b: only pairs where SST is in the range [5, 15]°C.

- C8c: only pairs where SST is $> 15°C$.
- C9a: only pairs where SSS is < 33.
- C9b: only pairs where SSS is in the range [33, 37].
- C9c: only pairs where SSS is > 37.

Table 1: Statistics of ΔSSS (Satellite - TSG-LEGOS-DM)

Condition	#	Median	Mean	Std	RMS	IQR	r^2	Std*
all	10400	-0.47	-0.63	0.64	0.89	0.67	0.00	0.46
C1	0	NaN	NaN	NaN	NaN	NaN	NaN	NaN
C2	7406	-0.54	-0.71	0.68	0.99	0.75	0.00	0.51
C3	103	-0.14	-0.11	0.32	0.34	0.59	0.07	0.44
C5	318	-0.37	-0.68	0.62	0.92	1.06	0.11	0.34
C6	10075	-0.47	-0.63	0.64	0.89	0.67	0.00	0.46
C7a	5019	-0.42	-0.57	0.60	0.83	0.64	0.00	0.43
C7b	5381	-0.50	-0.68	0.66	0.95	0.72	0.01	0.49
C7c	0	NaN	NaN	NaN	NaN	NaN	NaN	NaN
C8a	2395	-1.19	-1.22	0.75	1.43	1.04	0.02	0.88
C8b	4422	-0.50	-0.59	0.54	0.80	0.54	0.03	0.40
C8c	3583	-0.27	-0.28	0.28	0.40	0.34	0.34	0.25
C9a	81	0.46	0.46	0.34	0.57	0.27	0.03	0.22
C9b	10319	-0.47	-0.64	0.63	0.89	0.67	0.00	0.45
C9c	0	NaN	NaN	NaN	NaN	NaN	NaN	NaN

▶ Table 2 presents statistics of ΔSSS (Satellite - ISAS) using only ISAS SSS values with PCTVAR<80%.

Table 2: Statistics of ΔSSS (Satellite - ISAS)

Condition	#	Median	Mean	Std	RMS	IQR	r^2	Std*
all	9268	-0.44	-0.62	0.61	0.87	0.67	0.00	0.42
C1	0	NaN	NaN	NaN	NaN	NaN	NaN	NaN
C2	6724	-0.50	-0.70	0.65	0.95	0.83	0.01	0.51
C3	68	-0.30	-0.31	0.10	0.32	0.13	0.01	0.11
C5	318	-0.26	-0.68	0.61	0.92	1.40	0.26	0.10
C6	8949	-0.45	-0.62	0.61	0.86	0.67	0.00	0.43
C7a	3964	-0.39	-0.59	0.60	0.84	0.62	0.02	0.38
C7b	5304	-0.47	-0.64	0.61	0.89	0.69	0.00	0.45
C7c	0	NaN	NaN	NaN	NaN	NaN	NaN	NaN
C8a	2395	-1.10	-1.09	0.70	1.29	1.16	0.00	0.80
C8b	4021	-0.48	-0.61	0.54	0.81	0.56	0.01	0.42
C8c	2852	-0.21	-0.24	0.23	0.33	0.27	0.48	0.20
C9a	79	-0.21	-0.17	0.15	0.23	0.19	0.41	0.09
C9b	9189	-0.45	-0.62	0.61	0.87	0.68	0.00	0.43
C9c	0	NaN	NaN	NaN	NaN	NaN	NaN	NaN

▶ Numerical values can be downloaded as csv files for Table 1 and Table 2.

5 More Comparison/Validation Materials

5.1 Comparisons with other satellite products

► Table 1 shows the mean, median, standard deviation (Std), root mean square (RMS), interquartile range (IQR), correlation coefficient (r^2) and robust standard deviation (Std*) of the match-up differences ΔSSS (Satellite - TSG-LEGOS-DM) between different satellite products and **TSG-LEGOS-DM** derived over the Sea of Japan Pi-MEP region considering all match-up pairs satellite/*in situ* SSS values to derive the statistics:

Table 1: Statistics of ΔSSS (Satellite - *in situ*) - All

Satellite products	#	Median	Mean	Std	RMS	IQR	r^2	Std*
smos-l2-v662	1052	-3.77	-4.06	2.91	5.00	3.29	0.00	2.76
smos-l3-catds-ifr-v2-1d-05deg	22	6.30	6.28	0.06	6.28	0.08	0.00	0.07
smos-l3-catds-ifr-v2-1m-025deg	2011	1.05	0.10	8.56	8.56	8.47	0.00	6.53
smos-l3-catds-cpdc-v321-l2q	11	0.42	0.42	0.01	0.42	0.00	NaN	0.00
smos-l3-catds-cpdc-v317-10d-25km	25992	-0.33	-0.29	1.56	1.58	1.86	0.05	1.39
smos-l3-catds-cpdc-v317-1m-25km	31994	-0.14	-0.14	1.30	1.30	1.53	0.08	1.14
smos-l3-catds-locean-v4-9d	54645	0.19	0.25	0.96	1.00	0.98	0.11	0.72
smos-l3-catds-locean-v4-18d	54645	0.18	0.25	0.75	0.79	0.78	0.12	0.57
smos-l3-bec-oa-v1-9d	6017	-0.56	-0.55	0.94	1.09	1.01	0.01	0.76
smos-l4-catds-ifr-v2-1w	483	-1.47	-11.26	14.56	18.39	27.42	0.24	3.17
aquarius-l2-or-v5	4511	-1.08	-1.52	1.92	2.45	1.75	0.00	1.15
aquarius-l3-or-v5-7dr	18554	-1.05	-1.38	1.63	2.14	1.43	0.01	1.02
aquarius-l3-or-v5-1m	21540	-1.14	-1.42	1.38	1.98	1.20	0.00	0.89
aquarius-l3-or-v5-7dr-rain-mask	17921	-1.02	-1.35	1.63	2.11	1.39	0.01	1.00
aquarius-l3-or-v5-1m-rain-mask	21443	-1.12	-1.39	1.38	1.95	1.21	0.01	0.90
aquarius-l2-jpl-v5	2125	-0.54	-1.14	1.73	2.07	1.93	0.00	1.39
aquarius-l3-jpl-v5-7dr	3135	-0.47	-0.68	0.74	1.00	1.05	0.00	0.61
aquarius-l3-jpl-v5-1m	10400	-0.47	-0.63	0.64	0.89	0.67	0.00	0.46
aquarius-l4-iprc-v5-1w	16014	0.01	0.00	0.33	0.33	0.36	0.39	0.27
aquarius-l4-iprc-v5-1m	18849	-0.01	-0.02	0.32	0.32	0.34	0.38	0.25
smap-l2-rss-v4	17095	-0.52	-0.59	0.95	1.12	0.95	0.25	0.71
smap-l3-rss-v4-8dr	22701	-0.51	-0.60	0.59	0.84	0.67	0.39	0.47
smap-l3-rss-v4-1m	22723	-0.43	-0.49	0.47	0.69	0.59	0.53	0.43
smap-l2-jpl-v4.3	24663	-0.47	-0.60	1.78	1.88	1.59	0.08	1.17
smap-l3-jpl-v4.3-8dr	22934	-0.44	-0.39	0.79	0.88	0.68	0.36	0.51
smap-l3-jpl-v4.3-1m	23833	-0.24	-0.27	0.76	0.80	0.73	0.34	0.53
cci-l4-esa-merged-oi-v1.8-7dr	29114	0.04	0.15	0.80	0.81	0.89	0.01	0.64
cci-l4-esa-merged-oi-v1.8-30dr	28433	0.01	0.11	0.75	0.76	0.80	0.01	0.60

► Table 2 is similar to Table 1 but considering only match-up pairs where RR=0 mm/h, 3< U_{10} <12 m/s, SST>5°C, distance to coast > 800 km.

Table 2: Statistics of ΔSSS (Satellite - TSG-LEGOS-DM) - C1

Satellite products	#	Median	Mean	Std	RMS	IQR	r^2	Std*
smos-l2-v662	0	NaN	NaN	NaN	NaN	NaN	NaN	NaN
smos-l3-catds-ifr-v2-1d-05deg	0	NaN	NaN	NaN	NaN	NaN	NaN	NaN
smos-l3-catds-ifr-v2-1m-025deg	0	NaN	NaN	NaN	NaN	NaN	NaN	NaN
smos-l3-catds-cpdc-v321-l2q	0	NaN	NaN	NaN	NaN	NaN	NaN	NaN
smos-l3-catds-cpdc-v317-10d-25km	0	NaN	NaN	NaN	NaN	NaN	NaN	NaN
smos-l3-catds-cpdc-v317-1m-25km	0	NaN	NaN	NaN	NaN	NaN	NaN	NaN
smos-l3-catds-locean-v4-9d	0	NaN	NaN	NaN	NaN	NaN	NaN	NaN
smos-l3-catds-locean-v4-18d	0	NaN	NaN	NaN	NaN	NaN	NaN	NaN
smos-l3-bec-oa-v1-9d	0	NaN	NaN	NaN	NaN	NaN	NaN	NaN
smos-l4-catds-ifr-v2-1w	0	NaN	NaN	NaN	NaN	NaN	NaN	NaN
aquarius-l2-or-v5	0	NaN	NaN	NaN	NaN	NaN	NaN	NaN
aquarius-l3-or-v5-7dr	0	NaN	NaN	NaN	NaN	NaN	NaN	NaN
aquarius-l3-or-v5-1m	0	NaN	NaN	NaN	NaN	NaN	NaN	NaN
aquarius-l3-or-v5-7dr-rain-mask	0	NaN	NaN	NaN	NaN	NaN	NaN	NaN
aquarius-l3-or-v5-1m-rain-mask	0	NaN	NaN	NaN	NaN	NaN	NaN	NaN
aquarius-l2-jpl-v5	0	NaN	NaN	NaN	NaN	NaN	NaN	NaN
aquarius-l3-jpl-v5-7dr	0	NaN	NaN	NaN	NaN	NaN	NaN	NaN
aquarius-l3-jpl-v5-1m	0	NaN	NaN	NaN	NaN	NaN	NaN	NaN
aquarius-l4-iprc-v5-1w	0	NaN	NaN	NaN	NaN	NaN	NaN	NaN
aquarius-l4-iprc-v5-1m	0	NaN	NaN	NaN	NaN	NaN	NaN	NaN
smap-l2-rss-v4	0	NaN	NaN	NaN	NaN	NaN	NaN	NaN
smap-l3-rss-v4-8dr	0	NaN	NaN	NaN	NaN	NaN	NaN	NaN
smap-l3-rss-v4-1m	0	NaN	NaN	NaN	NaN	NaN	NaN	NaN
smap-l2-jpl-v4.3	0	NaN	NaN	NaN	NaN	NaN	NaN	NaN
smap-l3-jpl-v4.3-8dr	0	NaN	NaN	NaN	NaN	NaN	NaN	NaN
smap-l3-jpl-v4.3-1m	0	NaN	NaN	NaN	NaN	NaN	NaN	NaN
cci-l4-esa-merged-oi-v1.8-7dr	0	NaN	NaN	NaN	NaN	NaN	NaN	NaN
cci-l4-esa-merged-oi-v1.8-30dr	0	NaN	NaN	NaN	NaN	NaN	NaN	NaN

▶ Numerical values can be downloaded as csv files for Table 1 and Table 2.
▶ Figures using numerical values of Table 1 sorted by MEDIANS, MEANS, IQR, RMS, STD, R2 are also provided.
▶ Figures using numerical values of Table 2 sorted by MEDIANS, MEANS, IQR, RMS, STD, R2 are also provided.

Caution has to be made in the interpretation of the "ranking" between different satellite products in particular when looking at the dispersion parameters like the standard deviation (STD), or the interquartile range (IQR). Keep in mind that low spatial and/or temporal resolution satellite SSS products tend to have lower dispersions than products at higher resolutions. For example, a level 2 (swath) product of a specific sensor will always have more dispersion than level 3 or 4 products where spatial and temporal averaging tend to reduce the instrumental noise and potential small scale variability. In general, products at 1°x1° spatial resolution have lower dispersion than products at 0.25°x0.25°. Same result applies for monthly products compared to daily products.

5.2 Statistics derived for the different *in situ* databases

▶ Table 1 shows the mean, median, standard deviation (Std), root mean square (RMS), interquartile range (IQR), correlation coefficient (r^2) and robust standard deviation (Std*) of the match-up differences ΔSSS (Satellite - *in situ*) between **Aquarius-L3-JPL-V5-MONTHLY** and all the available *in situ* datasets derived over the Sea of Japan Pi-MEP region and for the full satellite product period and considering all match-up pairs satellite/*in situ* SSS values to derive the statistics:

Table 1: Statistics of ΔSSS (Satellite - *in situ*)

***in situ* database**	**#**	**Median**	**Mean**	**Std**	**RMS**	**IQR**	**r^2**	**Std***
argo	1259	-0.67	-0.77	0.72	1.06	0.92	0.02	0.66
tsg-legos-dm	10400	-0.47	-0.63	0.64	0.89	0.67	0.00	0.46

▶ Table 2 is similar to Table 1 but considering only match-up pairs where RR=0 mm/h, 3< U_{10} <12 m/s, SST>5°C, distance to coast > 800 km.

Table 2: Statistics of ΔSSS (Satellite - *in situ*)

***in situ* database**	**#**	**Median**	**Mean**	**Std**	**RMS**	**IQR**	**r^2**	**Std***
argo	0	NaN	NaN	NaN	NaN	NaN	NaN	NaN
tsg-legos-dm	0	NaN	NaN	NaN	NaN	NaN	NaN	NaN

▶ Numerical values can be downloaded as csv files for Table 1 and Table 2.

References

Gaël Alory, T. Delcroix, P. Téchiné, D. Diverrès, D. Varillon, S. Cravatte, Y. Gouriou, J. Grelet, S. Jacquin, E. Kestenare, and et al. The French contribution to the voluntary observing ships network of sea surface salinity. *Deep-Sea Res. Pt. I*, 105:1–18, November 2015. ISSN 0967-0637. doi: 10.1016/j.dsr.2015.08.005.

Abderrahim Bentamy and Denis Croize Fillon. Gridded surface wind fields from Metop/ASCAT measurements. *Int. J. Remote Sens.*, 33(6):1729–1754, March 2012. ISSN 1366-5901. doi: 10.1080/01431161.2011.600348.

Abderrahim Bentamy, Semyon A. Grodsky, James A. Carton, Denis Croizé-Fillon, and Bertrand Chapron. Matching ASCAT and QuikSCAT winds. *J. Geophys. Res.*, 117(C2), February 2012. ISSN 0148-0227. doi: 10.1029/2011JC007479. C02011.

Jaqueline Boutin, Y. Chao, W. E. Asher, T. Delcroix, R. Drucker, K. Drushka, N. Kolodziejczyk, T. Lee, N. Reul, G. Reverdin, J. Schanze, A. Soloviev, L. Yu, J. Anderson, L. Brucker, E. Dinnat, A. S. Garcia, W. L. Jones, C. Maes, T. Meissner, W. Tang, N. Vinogradova, and B. Ward. Satellite and In Situ Salinity: Understanding Near-Surface Stratification and Sub-footprint Variability. *Bull. Am. Meterol. Soc.*, 97(8):1391–1407, 2016. ISSN 1520-0477. doi: 10.1175/bams-d-15-00032.1.

Clément de Boyer Montégut, Gurvan Madec, A. S. Fischer, A. Lazar, and D. Ludicone. Mixed layer depth over the global ocean: An examination of profile data and a profile-based climatology. *J. Geophys. Res.*, 109(C12), December 2004. doi: 10.1029/2004jc002378.

Clément de Boyer Montégut, Juliette Mignot, Alban Lazar, and Sophie Cravatte. Control of salinity on the mixed layer depth in the world ocean: 1. General description. *J. Geophys. Res.*, 112(C6), June 2007. ISSN 0148-0227. doi: 10.1029/2006jc003953.

Ralph R. Ferraro. SSM/I derived global rainfall estimates for climatological applications. *J. Geophys. Res.*, 102(D14):16715–16736, 07 1997. doi: 10.1029/97JD01210.

Ralph R. Ferraro, Fuzhong Weng, Norman C. Grody, and Limin Zhao. Precipitation characteristics over land from the NOAA-15 AMSU sensor. *Geophys. Res. Lett.*, 27(17):2669–2672, 2000. doi: 10.1029/2000GL011665.

Fabienne Gaillard, E. Autret, V. Thierry, P. Galaup, C. Coatanoan, and T. Loubrieu. Quality Control of Large Argo Datasets. *J. Atmos. Oceanic Technol.*, 26(2):337–351, 2009. doi: 10.1175/2008JTECHO552.1.

Fabienne Gaillard, Thierry Reynaud, Virginie Thierry, Nicolas Kolodziejczyk, and Karina von Schuckmann. In Situ-Based Reanalysis of the Global Ocean Temperature and Salinity with ISAS: Variability of the Heat Content and Steric Height. *J. Clim.*, 29(4):1305–1323, February 2016. ISSN 1520-0442. doi: 10.1175/jcli-d-15-0028.1.

Robert J. Joyce, John E. Janowiak, Phillip A. Arkin, and Pingping Xie. CMORPH: A Method that Produces Global Precipitation Estimates from Passive Microwave and Infrared Data at High Spatial and Temporal Resolution. *J. Hydrometeorol.*, 5(3):487–503, June 2004. doi: 10.1175/1525-7541(2004)005⟨0487:camtpg⟩2.0.co;2.

Nicolas Kolodziejczyk, Gilles Reverdin, and Alban Lazar. Interannual Variability of the Mixed Layer Winter Convection and Spice Injection in the Eastern Subtropical North Atlantic. *J. Phys. Oceanogr.*, 45(2):504–525, Feb 2015. ISSN 1520-0485. doi: 10.1175/jpo-d-14-0042.1.

Christian Kummerow, Y. Hong, W. S. Olson, S. Yang, R. F. Adler, J. McCollum, R. Ferraro, G. Petty, D-B. Shin, and T. T. Wilheit. The Evolution of the Goddard Profiling Algorithm (GPROF) for Rainfall Estimation from Passive Microwave Sensors. *J. Appl. Meteorol.*, 40(11): 1801–1820, 2001. doi: 10.1175/1520-0450(2001)040⟨1801:TEOTGP⟩2.0.CO;2.